University of New Mexico
UNM Digital Repository

Fall 10-4-2016

APPLIED PHOTOPROPERTIES OF PHENYLENE ETHYNYLENES

Patrick L. Donabedian
University of New Mexico - Main Campus

Follow this and additional works at: https://digitalrepository.unm.edu/nsms_etds

Part of the Nanoscience and Nanotechnology Commons

Recommended Citation

Donabedian, Patrick L.. "APPLIED PHOTOPROPERTIES OF PHENYLENE ETHYNYLENES." (2016).
https://digitalrepository.unm.edu/nsms_etds/33

Patrick Lukins Donabedian

Candidate

Nanoscience and Microsystems Engineering

Department

This thesis is approved, and it is acceptable in quality and form for publication:

Approved by the Thesis Committee:

David Whitten , Chairperson

Eva Chi

David Keller

APPLIED PHOTOPROPERTIES OF PHENYLENE ETHYNYLENES

by

PATRICK L. DONABEDIAN

B.A. LIBERAL ARTS, ST. JOHN'S COLLEGE, 2012

THESIS

Submitted in Partial Fulfillment of the
Requirements for the Degree of

Master of Science
Nanoscience and Microsystems Engineering

The University of New Mexico
Albuquerque, New Mexico

December, 2016

Acknowledgements

I could not have done this without so many people. Dave's kindness and enthusiasm brought me into the fold at the beginning, and kept me going past many obstacles. Eva's commitment to her students and to excellent science pushed me to improve my work again and again, without losing sight of the responsibility of maintaining a safe, fun and educational lab. Ying was a tireless exemplar of the true scientist. Eric's creativity and complete disregard for social norms were an inspiration. Harry kept us all from taking ourselves too seriously, and taught me valuable lessons about both cytometry and sports words. Tom's many insights and quiet determination provided much wisdom. I have long since learned to underestimate Florencia at my peril, and I pin my hopes for the future on her. Arjun was always helpful, eager, and learned. Adeline's willingness to explain what she's doing taught me more molecular biology than a thousand lectures. Greg's companionship, and his mastery of circular dichroism, got me through more than one late night in the lab. Dr. Keller built worlds at the blackboard, and opened my mind to new frontiers: the wonders of statistical physics! Lance knew all of the secrets of AFM, if you could get him to stop talking about Zelda. And Suhyun, of course, has taught me more than anyone—not least, to pronounce her name properly.

I could not have had better friends and compatriots in this strange, accidental journey. I am sad and happy to be leaving them, and I will try to do justice to their gifts.

APPLIED PHOTOPROPERTIES OF
PHENYLENE ETHYNYLENES

by

Patrick L. Donabedian

B.A. Liberal Arts, St. John's College, 2012

M.S. Nanoscience and Microsystems Engineering, University of New Mexico, 2016

Abstract

Light-absorbing molecules can be used as powerful tools to perturb and understand biological systems by fluorescence, sensitization, or photochemical reactions. A thorough understanding of the delivery of dyes to specific biochemical targets and the processes that control the fate of excited-state energy is needed to engineer useful technology out of organic photochemistry. This thesis presents four projects investigating different aspects of pathogen destruction and biochemical sensing in a variety of systems, using the properties of p-phenylene ethynylenes (PEs), an especially flexible and well-studied class of conjugated molecules. Of particular relevance, some PEs are found to be effective dyes for amyloid protein aggregates both in solution and in mouse and human brain tissue. As well, control of the solvent microenvironment can be used to tune accessibility of the triplet state, which has implications for targeted photodynamic inactivation of both pathogens and cancer cells.

Table of Contents

I. Introduction

Fluorescent dyes are an essential tool in modern biology for their ability to resolve biological structures and processes in real time, and, in superresolved applications, with spatial resolution close to that of individual molecular phenomena. Multiple layers of space/time biological information can be collected from the same system by using multiple fluorescent markers, and a well-characterized fluorophore can read out very detailed information about its physical and chemical environment, making many dimensions of data available to the well-prepared biologist.[1,2] To be capable of generating biologically relevant information, fluorophores have to be meaningfully coupled to biological processes, whether by direct binding of ligand-fluorophores to relevant structures, by conjugated antibody-antigen binding, or by genetic methods such as the expression of intrinsically fluorescent proteins. Of these, the latter two have more biological specificity, while the first is more direct, easiest to implement and has the least variability.
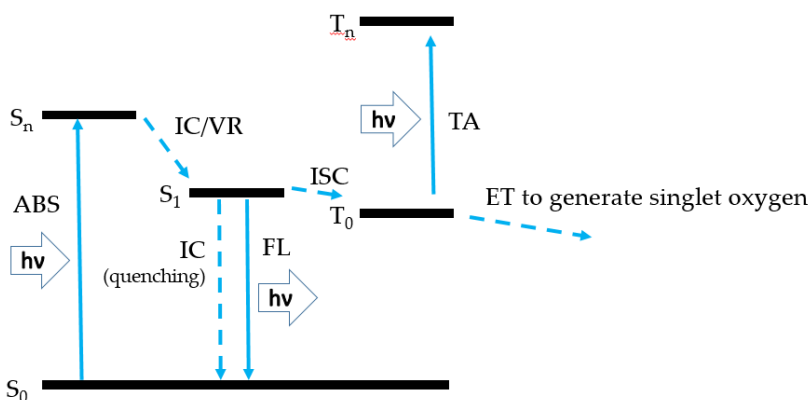
Figure I.1. Jablonski energy level diagram (vibrational transitions omitted) detailing the excitation and decay pathways relevant to the current discussion.

Non-emissive photoproperties of organic dyes have also found widespread applications in many fields, including biomedical research and technology. Leaving aside the extensive history of the process in film photography,[3] the generation of reactive singlet oxygen as a result of absorption of a quantum of light by a molecule has proven useful for destructive oxidation of

unwanted cellular systems, including cancer cells and microbial and viral pathogens. Photodynamic therapy exploits local dosing of a photosensitizer and local application of light irradiation to selectively destroy cancer cells, and has many advantages over other cancer therapies in cases where photoirradiation is convenient (i.e., cancers close to the surface of an easily exposed tissue).[4–6] The principles of cancer photodynamic therapy have been extended in recent years to microbial pathogens, giving rise to the field of antimicrobial photodynamic therapy.[7]

In the current thesis, we will examine four projects: synthesis of two minor variants of a cationic oligo(phenylene ethynylene) bearing different cationic rings and brief testing against bacteria; characterization of a subclass of solvent-sensitive OPEs as dyes for amyloid protein aggregates; extension of the OPE amyloid dyes to staining of brain tissue sections; and a spectroscopic exploration of triplet state populations in the solvent-sensitive dye class and their controllability by self-assembly with surfactants.

II. Synthesis of End-Functionalized OPEs

1. Background

Polymeric and oligomeric phenylene ethynylene electrolytes, especially those bearing cations, have been demonstrated to inactivate bacteria, pathogenic fungi and viruses through both light-dependent (photosensitization) and light-independent (membrane disruption) mechanisms, while leaving mammalian cells relatively unharmed.[8–11] Various configurations of cationic groups and conjugated backbone have been investigated, leading to the development of overall design principles. Cation-photosensitizers with a very short conjugated chain and cationic moieties at the ends, rather than the side-chains, have been shown to be effective against viruses and bacterial biofilms, and pathogenic fungal spores.[12–14] These "end-only functionalized" conjugated electrolytes' lesser bulk is hypothesized to allow them to diffuse into and disrupt viral capsid proteins and nucleic acids as well as the cellular components of biofilms. While these small compounds are more easily leached and photobleached than larger polymeric or oligomeric antimicrobials, their broad-spectrum inactivating ability against a variety of strategically important pathogens is greater.

In the first project to be discussed in this thesis, existing methods for synthesis of end-only functionalized cationic OPEs (EO-OPEs) were extended by the preparation of imidazolium and pyridinium derivatives of a triphenyl EO-OPE, named EO-IM and EO-PY. These derivatives were prepared after the improved antimicrobial performance of an imidazolium-functionalized poly(phenylene ethynylene) was demonstrated by Parthasarathy and Pappas.[9]
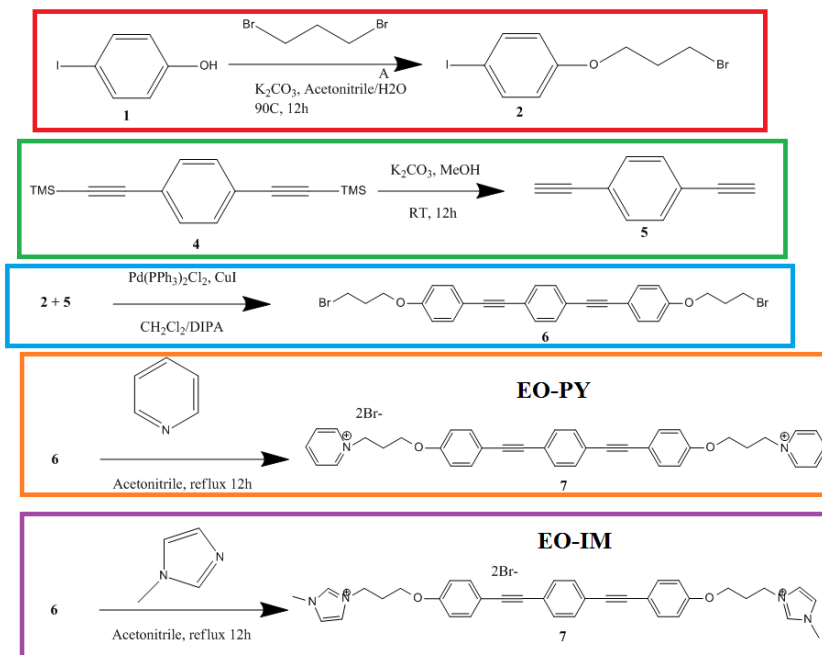
Figure II.1. Synthetic scheme used to prepare EO-PY and EO-IM.

2. Methods

Synthesis of OPEs was accomplished mostly by literature methods, as summarized in Figure II.1.[15,16] Briefly, OPE precursors were prepared and coupled by Sonogashira reaction catalyzed by $(PPh_3)_2PdCl_2$ and CuI in a degassed mixture of dichloromethane and diisopropylamine under Ar. The OPEs were prepared as a bromoalkyl ether, which was reacted with 1-methyl imidazole (for EO-IM) or pyridine (for EO-PY) to form the final product.

Synthesis of 1-(3-bromopropoxy)-4-iodobenzene (2): K2CO3 (12.4 g, 10 eq) was added to a stirring mixture of 40 mL acetonitrile with 5 mL of water in a round-bottomed flask in an oil bath, followed by 4-iodophenol (2 g, 9 mmol). The flask was fitted with a reflux condenser, the mixture heated to reflux and 1,3-dibromopropane (3.6 g, 1.8 mL, 2 eq) was added dropwise. After 12 hours at reflux, the excess base was removed by filtration and the reaction mixture washed with 1N HCl, saturated NaHCO3, and saturated brine, and extracted with dichloromethane. The organic fraction was removed, residual water removed by standing over MgSO4 for 30 minutes.

Dichloromethane was removed by rotary evaporation and excess 1,3-dibromopropane by standing in a watch glass overnight. Recovered 2.18 g of a white solid (71% yield).

Synthesis of 1,4-diethynylbenzene (5): 1,4-bis(trimethylsilyl)ethynylbenzene (1 g, 3.70 mmol) was added to a stirring solution of K2CO3 (5.1 g, 10 eq) in MeOH (40 mL). The solution was stirred for 5 h at room temperature, the excess base removed by filtration, and the solvent removed by rotary evaporation under reduced pressure. The residue was dissolved in dichloromethane and washed sequentially with 1N HCl, saturated NaHCO3 and saturated brine. Removal of solvent yielded 400 mg of 5 in 86% yield.

Synthesis of 1,4-bis((4-(3-bromopropoxy)phenyl)ethynyl)benzene (6): 5 (300 mg, 2.38 mmol) and 2 (1.95 g, 2.4 eq) were dissolved in 40 mL of a 1:1 mixture of dichloromethane and diisopropylamine, and Pd(PPh3)2Cl2 (66.8 mg, 4 mol %) and CuI (36 mg, 8 mol %) were suspended in 100 mL of a 1:1 mixture of dichloromethane and diisopropylamine which had been sparged with Ar for 20 minutes. Both solutions were sealed with rubber septa and sparged with Ar for 30 minutes, then cooled to 0ºC. The reactants were added to the catalyst suspension by cannula transfer under Ar pressure, and the reaction mixture was sealed with parafilm and fitted with a balloon providing positive pressure of Ar. After 12 hours, 40 mL of dichloromethane was added to the reaction mixture, the mixture was filtered and the solvent removed under reduced pressure. The bright orange residue was resuspended in dichloromethane and washed sequentially with saturated NH4Cl, saturated NaHCO3, and saturated brine. The organic layer was dried by MgSO4, solvent removed under reduced pressure and the residue chromatographed on silica using a 20:1 to 10:1 to 5:1 gradient of dichloromethane:methanol mixtures, yielding (197 mg, 15% yield).

Synthesis of EO-IM: 6 (50 mg, 0.09 mmol) was refluxed with 10 equivalents of 1-methylimidazole overnight in acetonitrile. Solvent was removed under reduced pressure and the liquid washed with water and dichloromethane, yielding 40 mg EO-PY in 80% yield.

Synthesis of EO-PY: 6 (50 mg, 0.09 mmol) was refluxed with 10 equivalents of pyridine overnight in acetonitrile. Both the solvent and excess pyridine were removed by long drying under reduced pressure. 40 mg of EO-PY was produced in 80% yield.

Effectiveness of EO-IM and EO-PY against populations of *S. aureus* was evaluated by live/dead stain flow cytometry. Bacterial cells were grown in nutrient broth, diluted to 1e6 cells/mL, and stock solutions of EO-IM, EO-PY and EO-DABCO added to a total concentration of 5 ug/mL. The three OPE samples and a control were incubated for 30 minutes under 350 nm UVA light in a photoreactor, stained with SYTO 9 and propidium iodide, and counted on a flow cytometer (Accuri C6). The gates used to determine live and dead populations were derived from previous control experiments using fresh incubated cells (live) and cells exposed to 70% EtOH overnight (dead). These experiments were only performed at one set of concentrations, and were not complete or conclusive.

3. Discussion & Conclusions

Figure II.2. ESI-MS exact mass spectrum of a sample containing EO-IM, indicating the presence of an m/z peak at 278.1426 for a mass of 556.2852, 2.5 parts per million off from the expected mass of 556.2838.
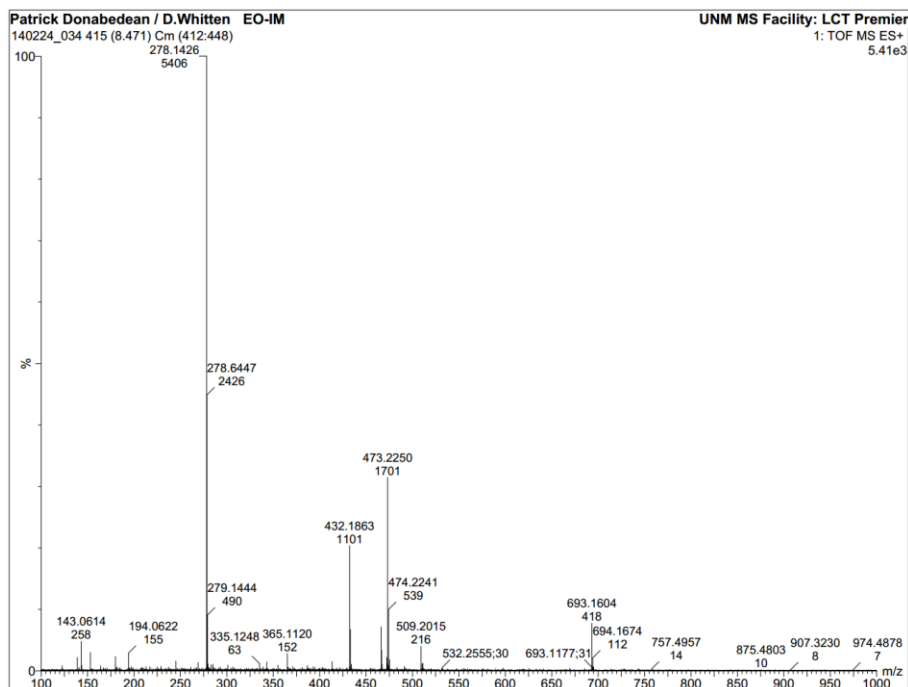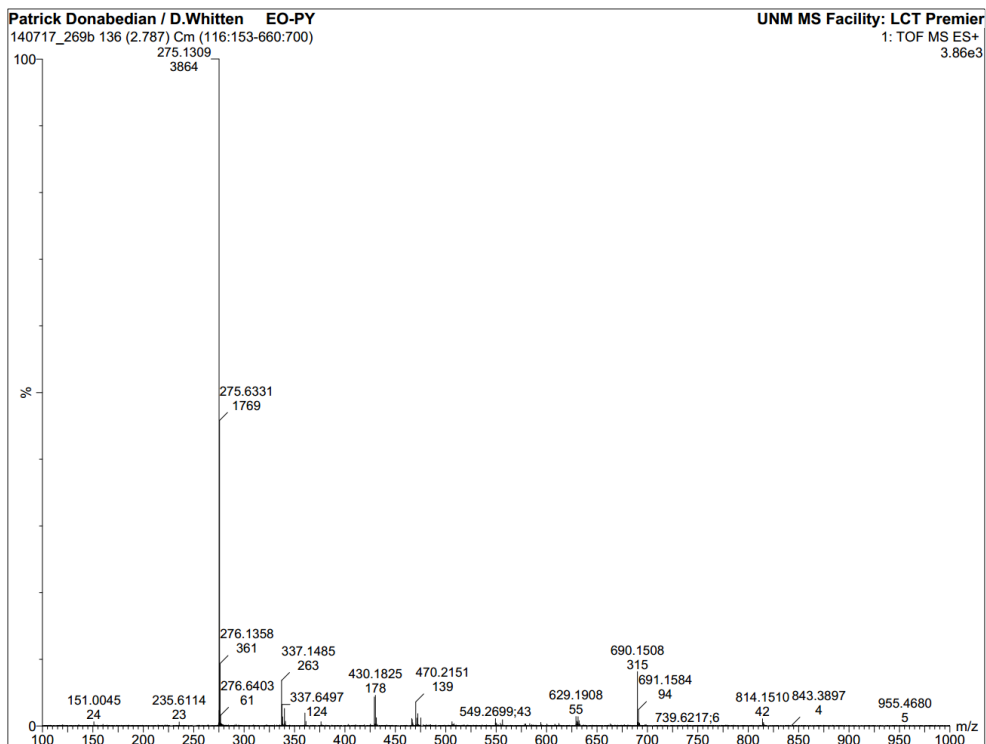
Figure II.3. ESI-MS exact mass spectrum of a sample containing EO-PY, indicating the presence of an m/z peak at 275.1309 for a mass of 550.2618, 0.4 parts per million off from the expected mass of 550.2620.
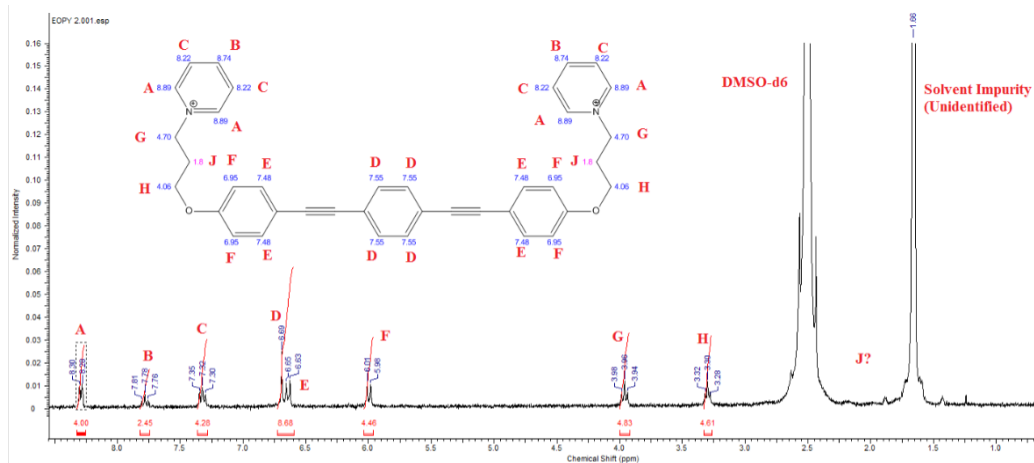
Figure II.4. Proton NMR spectrum of EO-PY with peak assignments and integration. The "unidentified" impurity is water.
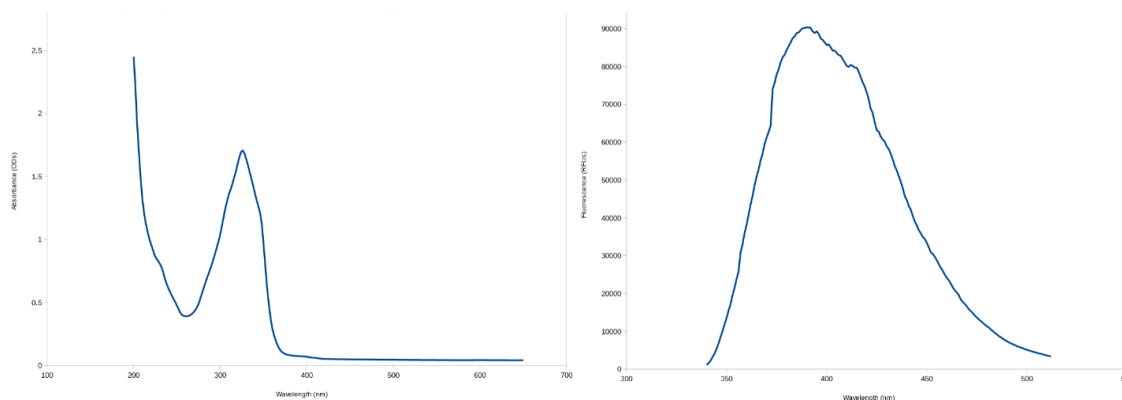
Figure II.6. Absorbance (left) and fluorescence spectra of EO-IM (those of EO-PY are identical). Fluorescence is plotted on an arbitrary scale, absorbance in OD.

^{1}H NMR and mass spectrometry of EO-IM and EO-PY (Figures II.2-4) indicated that the molecule was synthesized as intended and contained only trace impurities, with both molecular weight and molecular connectivity determined as expected. Absorbance and fluorescence of EO-IM is shown in Figure II.6, and is extremely similar to that of other EO-OPEs.
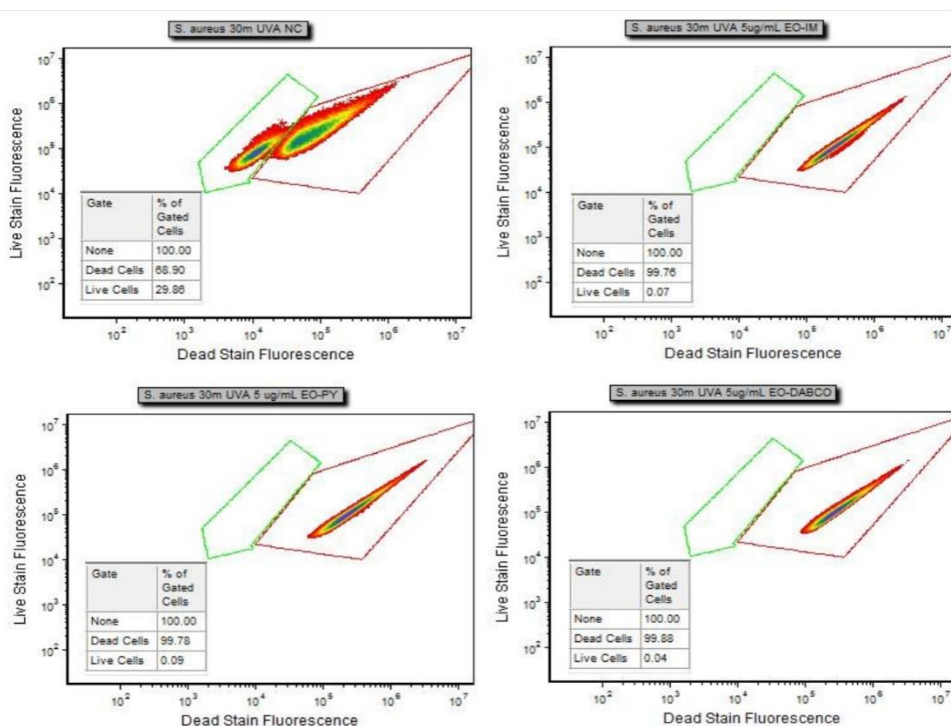
Figure II.7. Flow cytometric analysis of the *S. aureus* killing efficiency of EO-IM and EO-PY under 30m UVA irradiation, compared to that of EO-OPE-DABCO. All OPEs were applied at a concentration of 5 ug/mL.

EO-IM and EO-PY were found to be equally as effective as EO-DABCO at killing of *S. aureus* bacterial populations at the 5 ug/mL concentrations tested, with 99.8% of cells appearing "dead" compared to 68.9% for UVA control. Characterization of these compounds is incomplete. It is possible that the effectiveness of these compounds might vary significantly at different concentrations, or against different organisms. These compounds were synthesized in an attempt to explore the effect of different cationic groups on the antimicrobial effectiveness of different OPEs. A full exploration of these effects was not completed and drawing any conclusions would be premature. This work is included in this thesis in the hope that it might be continued in the future, and yield some useful information about the effect of the cation group on the behavior of these antimicrobial compounds.

III. Using a Desolvation Trigger and Steric Targeting with Amphiphilic Dyes: Sensing of Amyloids I

1. Background

The goal of this project is to develop new tools to improve the properties of biological dyes, focusing on binding-activated changes in photophysical properties such as quantum yields of fluorescence and photochemical sensitization. Amyloids are a class of beta-sheet-rich, linear peptide intermolecular homopolymers found in healthy and diseased states in many living systems.[17] Amyloids form the major component of plaques found in neurodegenerative diseases such as Alzheiemer's, Parkinson's, Huntington's and others,[18,19] the extracellular matrix secreted by Enterobacteria,[20] and deposits in the organs of some phenotypically healthy older people.[21] The exceptional thermodynamic stability of amyloids, as well as their ability to template the formation of further aggregates, forms the basis for transmission of prions, abiotic pathogens responsible for various transmissible spongiform encephalopathies such as kuru, Creutzfeldt-Jakob disease and bovine spongiform encephalopathy ("mad cow disease").[22] The rich and varied biochemistry of amyloids has been well-studied both due to their ostensible involvement in certain diseases of enormous economic importance and their susceptibility to detection by the binding of fluorescent dyes.

Regardless of the pathology, monitoring the course of amyloid formation at the biochemical, cellular and tissue levels, both in humans and animal models, is vital to understanding and combating AD and other proteinopathies[23]. Though conformation- and sequence-specific antibodies have been developed for amyloid applications[24], the primary means of detecting and localizing amyloid aggregates are small-molecule probes, whether fluorescent ligands, radiolabeled ligands for positron-emission tomography (PET)[25] and single photon

emission computed tomography (SPECT), or metal-ligated magnetic resonance imaging (MRI) contrast agents[26]. Fluorescent ligands are especially attractive because of their inherently lower capital costs, lack of radioactivity and the detailed chemical and structural information that can be extracted from the spectral properties of a bound molecule. A variety of chemical and photophysical properties may be desirable in an amyloid fluorescent biomarker. First, the compound must bind to the amyloid fibril protein conformation with high affinity and specificity. Compounds that bind specifically to amyloid tend to share a common molecular profile with a "rigid conjugated rod" morphology; computational studies have shown that linear shape and aromaticity are favorable for binding to hydrophobic surface grooves in the amyloid fibril[27]; similar binding modes have been supported by scanning tunneling microscopy[28]. Past studies of amyloid-specific probes have investigated molecular scaffolds derived[29] from Congo red/curcumin[30–32], Thioflavin T[33–35], oligothiophenes[21,36–41], or other scaffolds[42–44]. These ligands, when used for fluorescent imaging, primarily function on a "molecular rotor" basis, in which fluorescence enhancement and emission redshift is accomplished by planarization of the conjugated region and prevention of rotation within the fluorophore when bound to a planar site on the amyloid fibril surface. Studies have targeted various properties, such as murine *in vivo* imaging, detection of pre-thioflavinophilic amyloids, structural differentiation of amyloids with different precursors or properties, two-photon imaging or near-infrared excitation and emission.

A useful fluorophore for most applications *ex vivo* should have optical transitions within the range of commercially available laser lines and detectors, large extinction coefficient, and bright, slowly-bleaching fluorescence. For ligand-fluorophores, the most desirable properties are strong selective binding to the target structure and, ideally, an increase in quantum yield of fluorescence in the bound vs. free state. The first property, that of selective binding, is already difficult to tune for, but is primarily the result of sterics, electrostatic and hydrophobic matching to a target site. The second property is even less well-understood and developed from a design standpoint, being the result of physically complex properties of ligand electronic structure. This

project comprised an attempt to integrate both properties following the fortuitous discovery of a binding-triggered fluorescence yield change associated with desolvation in an ethyl ester-functionalized subclass of phenylene ethynylene electrolytes.

In 2011, Tang et al[45] discovered an unexpected property of their newly synthesized p-phenylene ethynylene oligomers: While unfunctionalized p-phenyleneethynylenes had similar quantum yields of fluorescence in water and in methanol, the molecules with phenylene-attached ethyl esters had drastically reduced fluorescence yields in water. This property was noted and given some cursory explanation in their original paper, and subsequently used in self-assembling sensor systems for various enzymes by Hill[46]. Through a poorly-understood mechanism, excited states are able to decay to ground through non-radiative energy transfer to solvent, a process which is most efficient for H_2O and less efficient in less strongly H-bonding solvents. This solvent-sensitive fluorescent emission property serves as a "desolvation trigger" that lights up the dye fluorescence upon binding to protein aggregates.

2. Methods

Except OPEs, all reagents were obtained commercially and used without further purification. Synthesis of OPEs has been reported previously[45], except for OPE1-, which was synthesized analogously to OPE1+. Hen egg white lysozyme (HEWL), Thioflavin T and buffer components were obtained from Sigma-Aldrich Chemical Company (St. Louis, MO). All water was purified with a Synergy UV Millipore purification system (EMD Millipore, Billerica, MA). Suspensions of protein aggregates were gently vortexed to distribute aggregates before use in experiments.

Lyophilized HEWL was dissolved at 10 mg/mL (700 μM) in 10 mM pH 3 sodium citrate buffer with 0.1 M NaCl. The solution was incubated in a 70°C oil bath and magnetically stirred at 250 rpm for 12h, and aliquots were withdrawn at half-hour intervals. The initially clear solution was observed to form cloudy aggregates by 1h of incubation. Half of each aliquot was

immediately diluted into pH 7.4 phosphate buffer to prevent further influence of acidic conditions and stored at 4C. The samples were observed to undergo no noticeable degradation over the course of one month, and these neutralized aliquots were used for all following experiments except for measurements of protein circular dichroism.

For studies of fluorescence enhancement vs. protein incubation time, dyes were mixed with protein sample in phosphate buffer (PB, 10 mM, pH 7.4) at an equal monomer concentration of 10 μM in the wells of a standard 96-well plate. Emission spectra were obtained using a SpectraMax M2e plate-reading spectrophotometer (Molecular Devices, Sunnyvale, CA). Experiments were performed in duplicate and errors are reported as standard deviation. For analysis of bound OPE excitation and emission spectra and protein-OPE energy transfer, OPEs (500 nM) were mixed with protein sample (5 μM, monomer basis) in PB and the solution transferred to a quartz fluorometry cuvette. Spectra were obtained on a PTI QuantaMaster 40 steady state spectrofluorometer (HORIBA Scientific, Edison, NJ).

For protein intrinsic circular dichroism, protein samples were diluted in sodium citrate buffer without NaCl (pH 3, 10 mM) to a concentration of 0.14 mg/mL, gently vortexed, and read in a 1mm pathlength quartz CD cuvette using an Aviv 410 CD spectrometer (Aviv Biomedical, Lakewood, NJ) with a 15s averaging time. A blank spectrum (PB only) was subtracted from each sample to remove background signal. Error bars are standard deviation over multiple reads of a single sample as reported by the instrument.

For OPE induced circular dichroism, OPEs and protein were diluted in phosphate buffer (pH 7.4, 10 mM) to an OPE and protein concentration of 5 μM, and data was obtained and processed identically to the protein CD experiments.

For determination of binding constant of OPEs to amyloid aggregates, OPEs were mixed with HEWL amyloid in PB at a final OPE concentration ranging from 100 nM to 5 μM and final protein concentration of 5 μM (monomer basis). The solutions were then transferred to a quartz fluorometry cuvette and emission measured at the pertinent wavelength. Experiments were

performed in duplicate and errors reported as standard deviation. Hill function fits to OPE binding curves were calculated using OriginPro 9.

For AFM, a droplet of each protein sample at 5 mg/mL was pipetted onto freshly cleaved mica substrate and allowed to physisorb for 20 min, followed by a single rinse with HPLC-grade water and gentle drying under a stream of N_2. Imaging was performed with a Nanoscope IIIa AFM (Veeco, Plainview, NY) in tapping mode under a constant stream of dry N_2 gas using a rectangular silicon cantilever with a spring constant of 40 N/m (Veeco model RTESPA-W). Veeco Nanoscope software was used to capture and analyze the images. 0h and 1h images are cropped from 1 μm width images subjected to a first-order x,y plane fit and flattened. 1.5h image is cropped from a 5 μm width image subjected to a third-order x,y plane fit and flattened. 4h image is cropped from a 5 μm width image subjected to a first-order x,y plane fit.

For TEM imaging, incubated HEWL solutions at a concentration of 350 μM were diluted 1:5 in water and aliquoted onto carbon-coated grids, allowed to adsorb, washed with deionized water and stained with 2% uranyl acetate solution. Excess liquid was removed and the samples allowed to dry in air. Samples were imaged on a Hitatchi H7500 transmission electron microscope (Hitachi High Technologies Corp., Tokyo, Japan) with tungsten filament illumination, operating with an AMT X60 bottom mount CCD camera detector.

3. Discussion & Conclusions

Oligo(p-phenyleneethynylene) electrolytes (OPEs), which have been previously investigated along with their polymeric derivatives for a variety[47,48] of antimicrobial[11,49–51] and sensing[52–55] applications as well as for organic semiconductor devices, have many of the desirable properties for amyloid biomarkers, such as linear, highly conjugated morphology and several well-characterized fluorescence sensing effects. In addition to the molecular-rotor motif, OPEs can form supramolecular aggregates of different types[56] with distinct spectral characteristics, such as J aggregates. J, or Jelley, aggregation is a mode of dye complexation with characteristic

bathochromic absorbance shifts, sharpened fluorescence bands, enhancement of fluorescence yield and narrowed Stokes shift. These aggregates have a long history in dye chemistry, and recent reviews[57] can provide more detailed background. The exact structure of J-type aggregates varies somewhat with the dye and "brickwork," "ladder," and "staircase"-type arrangements have all been proposed[57]. OPEs with charged moieties pendant on the sides of the phenylene ethnylene (PE) backbone, rather than the ends, have been previously found to preferentially form J aggregates when complexed with oppositely charged surfactants[56]. In addition, ethyl ester termini have been shown to confer strong excited-state quenching of fluorescence by water: quantum yield of a cationic OPE with symmetric ethyl ester termini (OPE1+, Figure III.1) increases from 2.3% in water to 5% in deuterium oxide[58] and over 75% in methanol[45] (Table III.1). This effect vanishes when the ester is converted to a free carboxylate, and could be due to a hydrogen bonding or partial proton transfer mechanism[58]. These various effects give OPEs several distinct ways to provide spectral information about their environment and conformation, stemming from the one degree of rotational freedom in the ethynyl-aryl bonds, several different solvent quenching effects, Coulombic interactions with the charged groups and hydrophobic interactions with the conjugated backbone. These molecular and optical properties, and their similarity to the "rigid conjugated rod" morphology, led us to test OPEs as selective optical sensors for amyloids. In the present study, we selected four OPE molecules (Figure III.1) with ethyl ester termini and varying charge and number of repeat units, and successfully applied them *in vitro* as fluorescent probes specific for model amyloids formed from hen egg white lysozyme.

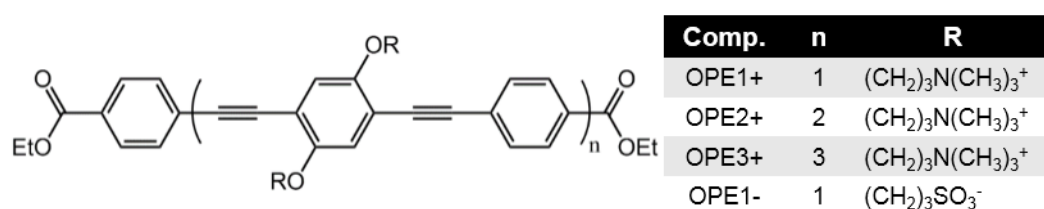| Comp.	n	R
OPE1+	1	$(CH_2)_3N(CH_3)_3^+$
OPE2+	2	$(CH_2)_3N(CH_3)_3^+$
OPE3+	3	$(CH_2)_3N(CH_3)_3^+$
OPE1-	1	$(CH_2)_3SO_3^-$

Figure III.1. Structure and functional groups of OPEs used in this study.

Four OPEs (Figure III.1) were chosen from our library of compounds for evaluation against HEWL amyloids. The OPEs used, designated for brevity OPEn+ and OPE1-, all have ethyl ester terminal moieties on the PE backbone and charged side-pendant groups; the cationic compounds have n = 1, 2 and 3 repeat units and the anionic compound has one repeat unit. The compounds are amphiphilic and water soluble due to the hydrophobic backbone and charged side groups. These ester-terminated compounds were selected for the effective sensing modality of fluorescence yield increase from reduced quenching by water when bound to a hydrophobic surface.

Formation and Characterization of HEWL Amyloids

Hen egg white lysozyme (HEWL) was used to form fibrillar amyloid aggregates for use in this study. Lysozyme has been suggested[59] as a useful model protein for amyloid studies, due to its low cost and the relative ease with which it can be induced to form amyloid aggregates. Lysozyme amyloid oligomers and fibrils have also been shown to exhibit cytotoxicity towards human neuroblastoma cells[60], indicating that the amyloid-aggregate conformer of lysozyme recapitulates most of the relevant properties of known disease-associated proteins. For our experiments, HEWL (Sigma-Aldrich) was incubated at 70˚C and a concentration of 350 μM in pH 3 sodium citrate buffer (10 mM) with 100 mM NaCl[61]. Visible precipitates of aggregated lysozyme were observed to accumulate over the time of incubation, and the formation of amyloid fibrils was characterized by Thioflavin T (ThT) fluorescence assay, far-UV circular dichroism (CD) spectroscopy, and atomic force microscopy (AFM) and transmission electron microscopy (TEM).
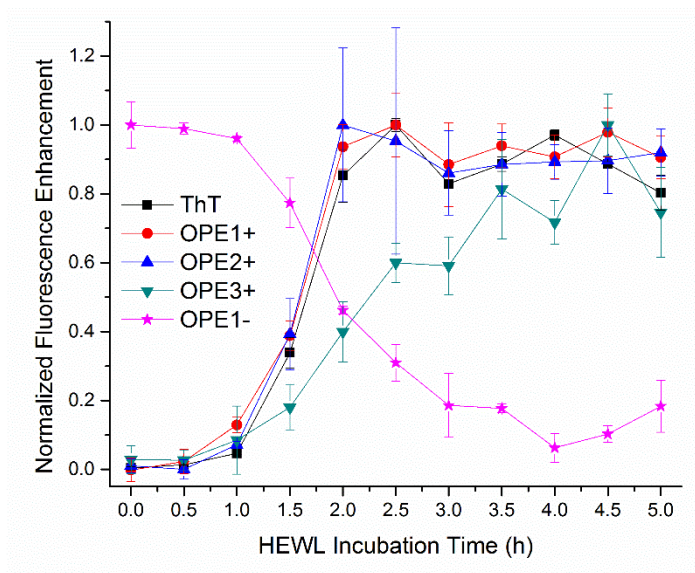
Figure III.2. OPE and Thioflavin T (10 μM) fluorescence enhancement profiles of HEWL incubated for various times (10 μM monomer basis, 0.5 mg/mL), with unbound dye fluorescence normalized to 0 and maximum dye fluorescence normalized to 1.
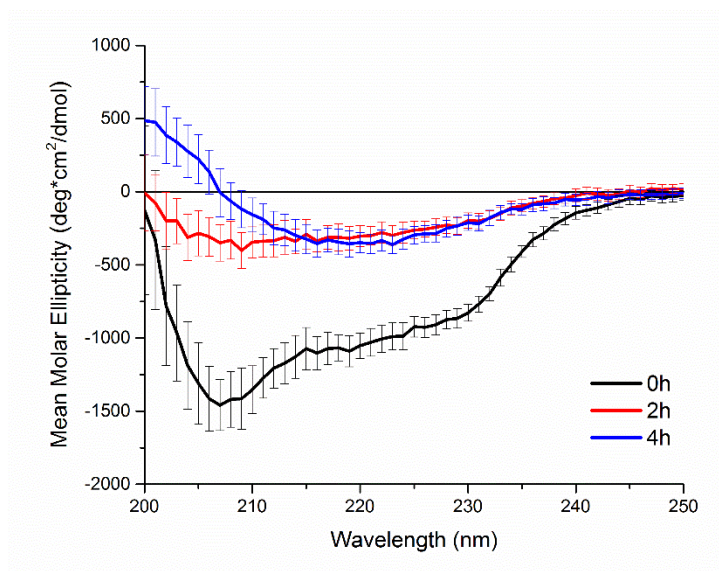
Figure III.3. Far-UV circular dichroism spectra of 0h, 2h and 4h incubated HEWL (0.14 mg/mL) in pH 3 citrate buffer (10 mM).

ThT-positive aggregates were detected by the second hour of incubation (Figure III.2), and the profile of ThT fluorescence enhancement over incubation time had the sigmoidal shape

consistent with the nucleation-controlled aggregation mechanism that is well accepted for amyloid formation. Far-UV CD measurements (Figure III.3) showed conversion of primarily α-helix structure of monomeric lysozyme (0h), as indicated by the negative bands at 222 and 208 nm, into primarily β-sheet structure in the mature aggregates (2h and 4h), as indicated by the single negative band at 218 nm and the positive band just visible at the 200 nm edge of the spectrum[62].
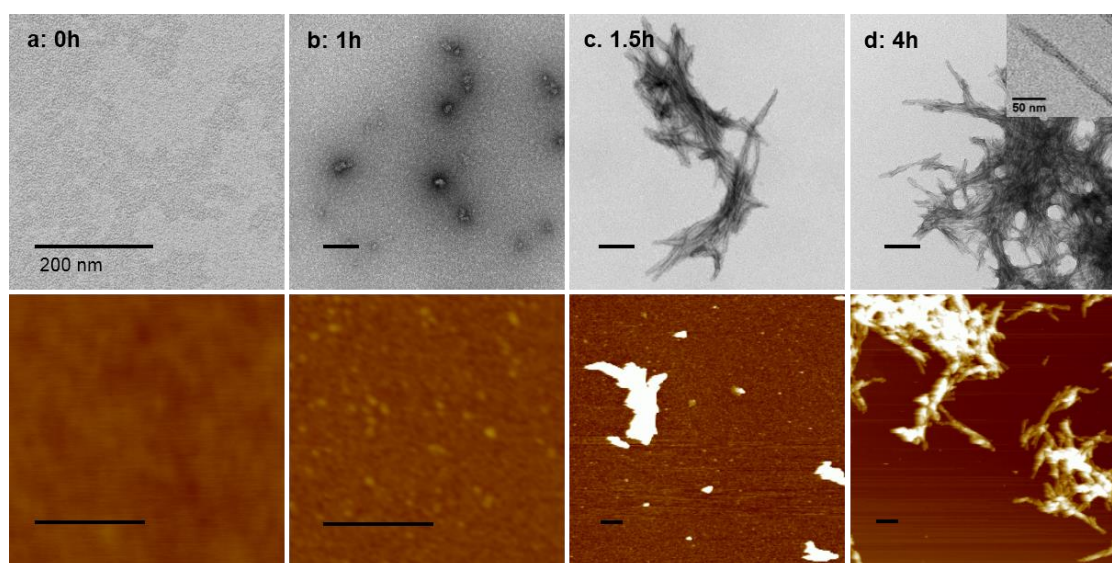
Figure III.4. TEM (top) and AFM (bottom) images of 0h (a), 1h (b), 1.5h (c) and 4h (d) incubated HEWL. Scale bars = 200 nm. 4h, inset: view of a single fibril, showing a twisted morphology. AFM image Z-height: 0h, 25 nm; 1h, 25 nm; 1.5h, 15 nm; 4h, 100 nm.

Fibrillar morphology of HEWL aggregates was visualized directly by AFM and TEM. AFM on dry mica and TEM (Figure III.4) on non-glow discharged carbon grids showed that unincubated HEWL (0h, Figure III.4a) formed a homogeneous film without large features. One hour of incubation (Figure III.4b) caused the HEWL to form distinguishable bumps, hypothesized to be pre-thioflavinophilic oligomers. By 1.5 hours of incubation when amyloid formation was just reaching the plateau phase as indicated by ThT fluorescence (Figure III.2), small linear aggregates were observed (Figure III.4c), which lengthened by the fourth hour into short, bundled fibrils 20-30 nm wide and 60-200 nm long (Figure III.4d). No fibrils significantly longer than

these were observed, even for longer incubated samples. These fibrillar, β-sheet enriched, ThT-positive HEWL amyloid aggregates were then used to evaluate the binding activity and photophysical changes of OPEs against amyloid.

Spectrophotometry of OPE-HEWL Interactions

Excitation and emission spectra of OPEs in phosphate buffer (PB) alone, with monomeric HEWL and with HEWL amyloids (8h incubated) are shown in Figure III.8, and relevant photophysical properties are summarized in Table 1. A 10:1 molar ratio of protein to OPE was used for these experiments. Absorbance spectra were also taken (Figure III.5) but background light scattering from insoluble amyloid aggregates made them difficult to interpret, so "fluorescence detected absorbance" in the form of excitation spectra was used instead. Normalized excitation and emission spectra, in which peak shifts and lineshape changes of spectra are easier to visualize, are provided in the Supporting Information (Figures III.6 and III.7). All four OPEs exhibited significant fluorescence enhancement in solution with HEWL amyloids (Figs. III.8e, f, g, h), and no fluorescence change with HEWL monomers except for OPE1-. The fluorescence enhancement over baseline was most significant for the longer OPE2+ and OPE3+ (Figs. III.8g and h), which also had notably sharpened fluorescence spectra with small (~10 nm) blueshifting of the maximum (Figure III.7). OPE1- had a similarly sharpened and blueshifted emission spectrum (Fig. III.8f and III.7) with both HEWL monomers and amyloid, with the appearance of a shoulder at 465 nm with amyloid. OPE1+ (Fig. III.8e) exhibited no change in wavelength or lineshape of emission spectrum, just a large increase in intensity when mixed with amyloids. The excitation spectra (Figs. III.8a, b, c, d) show a notable bathochromic shift for each OPE in solution mixed with amyloid, of 23, 27, 35 and 29 nm of the low-energy band for OPE1+, OPE2+, OPE3+ and OPE1-, respectively. The high-energy band, less relevant for imaging purposes, was also bathochromically shifted. Very small to no changes in excitation and emission were observed for the cationic OPEs when mixed with monomeric HEWL. The

anionic OPE1- had similar excitation spectrum (Fig. III.8b) when mixed with monomer and

amyloid, except for a moderate increase in intensity with amyloid.
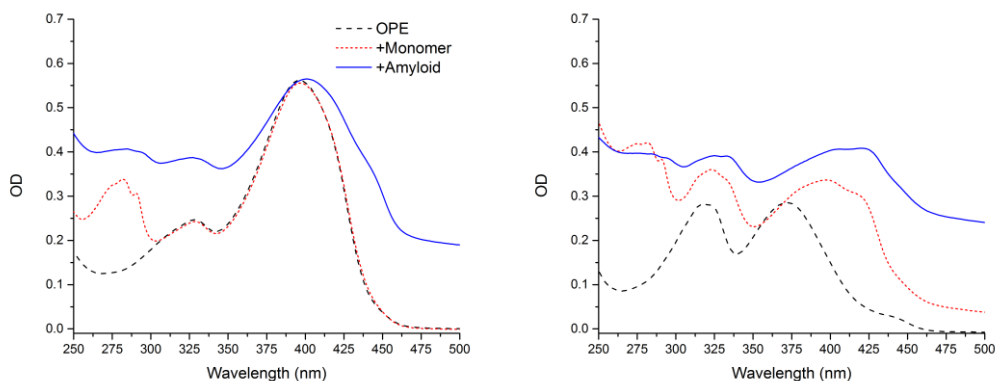
Figure III.5. Absorption spectra of OPE3+ (left) and OPE1- (5 µM) in PB alone (long dashed black line) with HEWL monomer (0.25 mg/mL) (short dashed red line) and with HEWL amyloid (9h aggregates, 0.25 mg/mL) (solid blue line). Scattering from insoluble aggregates appears as a large "white" absorption that obscures spectral features. Peak at 280 nm is HEWL native absorption.
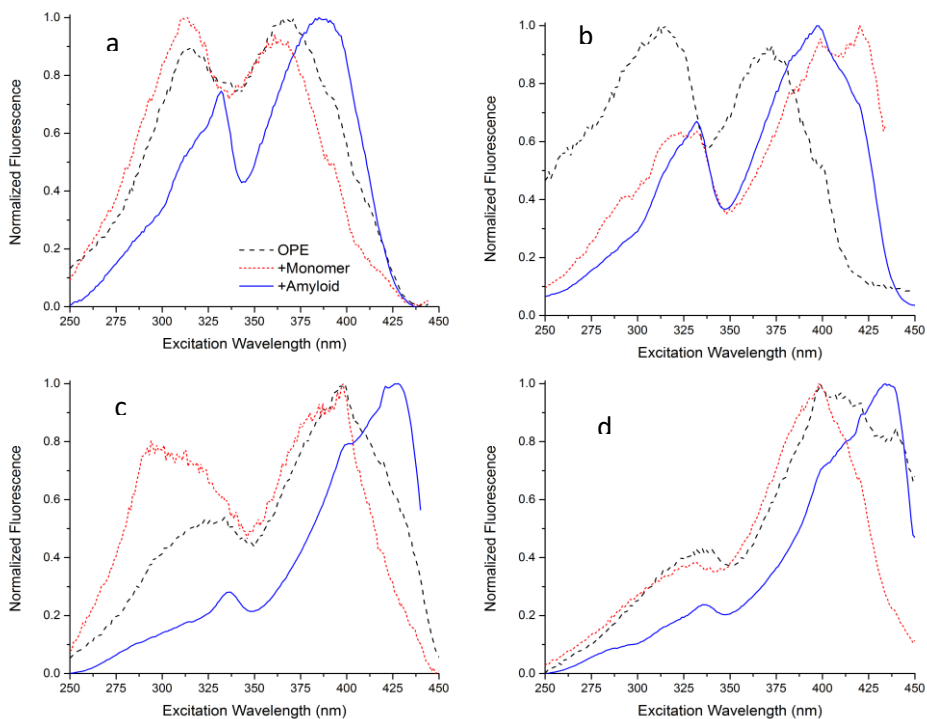
Figure III.6. Normalized excitation spectra of OPEs (a: OPE1+, b: OPE1-, c: OPE2+, d: OPE3+). Long dashed black line: OPE in PB alone. Short dashed red line: OPE in PB w/ HEWL monomers. Solid blue line: OPE in PB w/ HEWL amyloid (9h). OPE concentration = 500 nM, protein concentration 5 µM monomer basis / 0.25 mg/mL.
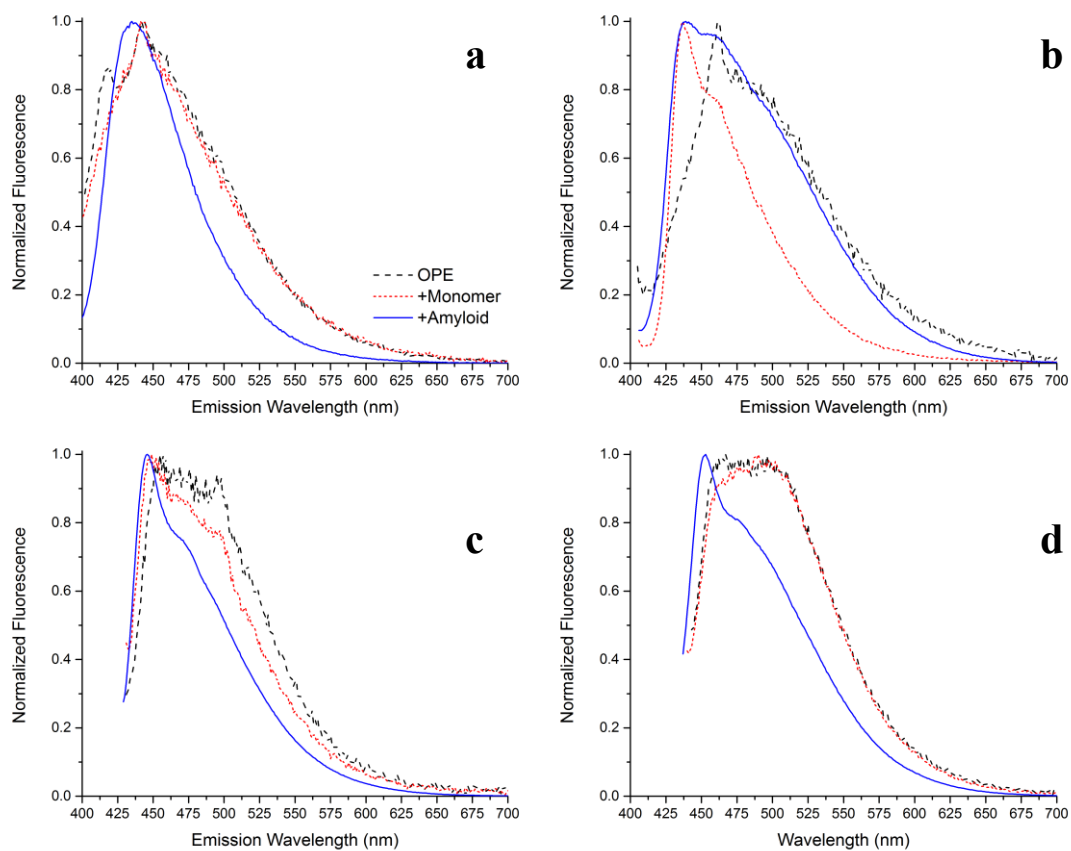
Figure III.7. Normalized emission spectra of OPEs (a: OPE1+, b: OPE1-, c: OPE2+, d: OPE3+). Long dashed black line: OPE in PB alone. Short dashed red line: OPE in PB w/ HEWL monomers. Solid blue line: OPE in PB w/ HEWL amyloid (9h). OPE concentration = 500 nM, protein concentration 5 μM monomer basis / 0.25 mg/mL.

| Comp.	Quantum Yield φ_{fl}[a]		Excitation Wavelengths λ_{ex} (nm)		Emission Wavelength λ_{em} (nm)			K (μM)	Hill Coeffi. n
	H$_2$O	MeOH	PB	PB with HEWL amyloids	H$_2$O	PB	PB with HEWL amyloids		
OPE1+	0.023	0.75	314, 362	332, 385	454	454	454	2.63 ± 0.58	1.04
OPE2+	0.039	0.71	330, 399	337, 426	448	460	445	1.15 ± 0.26	1.15
OPE3+	0.069	0.70	340, 399	335, 434	440	464	453	0.858 ± 0.058	1.89
OPE1-	-	-	314, 370	327, 399	454	454	439[b]	-	-

Table III.1. Relevant photophysical properties of OPEs alone and bound to HEWL amyloid, and apparent binding constants (K) and Hill coefficients (n) of OPE binding to HEWL amyloid. [a]From a previous study[56]. [b]Same maximum with monomer and amyloid, with the addition of a shoulder ~465nm with amyloid.
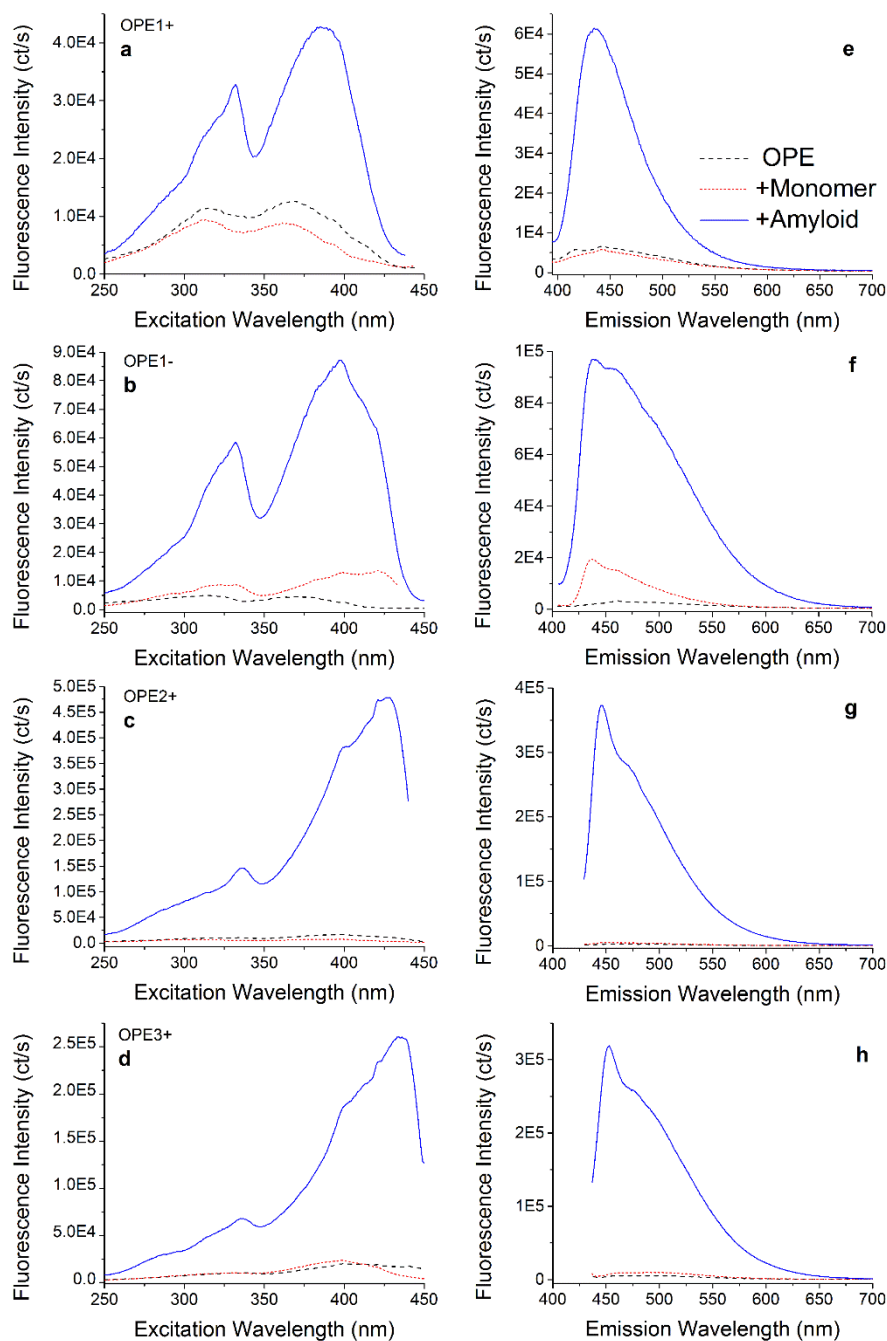
Figure III.8. Excitation (left; a, b, c, d) and emission (right; e, f, g, h) spectra of OPES (a, e: OPE1+; b, f: OPE1-; c, g: OPE2+; d, h: OPE3+) in phosphate buffer (PB, pH 7.4, 10 mM) alone (black long dashed line) with HEWL monomers (red short dashed line) and with HEWL amyloids (blue solid line). OPE concentration: 500 nM, protein concentration: 5 μM monomer basis / 0.25 mg/mL. Emission and excitation wavelengths, respectively, were chosen as shown in Table III.1 for each sample.

A plot of normalized fluorescence enhancement for all four OPEs and Thioflavin T with

HEWL fibrils incubated for different lengths of time is shown in Figure III.2. At a 1:1

protein:OPE molar ratio, OPE1+ and OPE2+ track amyloid formation in roughly the same way as

ThT, showing a sigmoidal curve with onset of a logarithmic growth phase occurring at the same

time, around 1h of incubation. The plateau phase, as monitored by fluorescence of any of those

three OPEs or ThT, appeared at 2 hours incubation. OPE3+ fluorescence enhancement shows a

similar length lag phase but a less sharp growth phase, taking up to 3.5 hours to reach its plateau

phase. At the equimolar concentrations used for this assay, OPE1- has greater fluorescence

enhancement when mixed with monomeric species than with amyloid, giving it a profile that is

the reverse of those observed for the cationic OPEs or ThT; this effect will be discussed below.

Determination of OPE/Amyloid Binding Constants

Next, binding saturation assays were conducted to quantify the affinity of OPE-amyloid

binding; data and fitted curves are shown in Figures III.9 and III.10 and the fitted parameters are

summarized in the last two columns of Table III.1. Since the linear fibril binding sites could

potentially fit many OPEs, binding curves were fitted to the Hill equation to capture possible

binding cooperativity:

$$y = \frac{F_{max}x^n}{K^n + x^n} \qquad \text{(Equation 1)}$$

where, y is OPE fluorescence intensity, x is OPE concentration (protein concentration was fixed

in these assays), F_{max} is OPE fluorescence intensity at saturation, K is the equilibrium dissociation

constant and the exponential term n is the Hill parameter which describes cooperativity of

binding[63]. n=1 indicates non-cooperative, independent binding, n>1 indicates that the binding of

one ligand increases affinity of the binding of a second (positive cooperativity), and n<1 indicated

that binding of one ligand decreases affinity of the binding of a second (negative cooperativity).

Fits to the data for the three cationic OPEs produced F_{max} values close to the observed

fluorescence saturation values, and fitted values of the other two parameters, K and n, are

reported in Table III.1 as calculated. The fits indicated that OPE1+, OPE2+ and OPE3+ bound to

HEWL amyloid with low micromolar affinity dependent on OPE length, with the calculated

dissociation constant decreasing from 2.6 μM for OPE1+ to 1.15 μM for OPE2+, and still further

to 858 nM for OPE3+. Furthermore, the cooperativity of OPE binding increased from almost no

cooperativity for OPE1+ (n=1.04), to some positive cooperativity for OPE2+ (n=1.15), to still

more positive cooperativity for OPE3+ (n=1.89). The quantitative physical meaning of the Hill

parameter is not quite clear except in special cases, but in a general way it is possible to conclude

that for the cationic OPEs, the shortest OPE has non-cooperative binding to HEWL amyloid (i.e.,

Michaelis-Menten binding), and the two longer OPEs have increasingly positively cooperative

binding.

Because the anionic OPE1- showed fluorescence changes with both monomeric and

fibrillar HEWL, binding assays were conducted for both conformers of HEWL. In contrast to the

binding curves of cationic OPEs, the binding of anionic OPE1- to HEWL monomers appeared to

be linear and non-saturable for up to 10 μM OPE concentration, or a 2:1 OPE:HEWL molar ratio,

indicating a low-affinity binding to a very large number of sites. Non-specific OPE1- binding to

HEWL monomers precluded accurate determination of a binding constant for OPE1-/amyloid

interactions (Supporting Information Figure III.10) such that quantitative comparisons of binding

between the cationic and anionic compounds cannot be made.
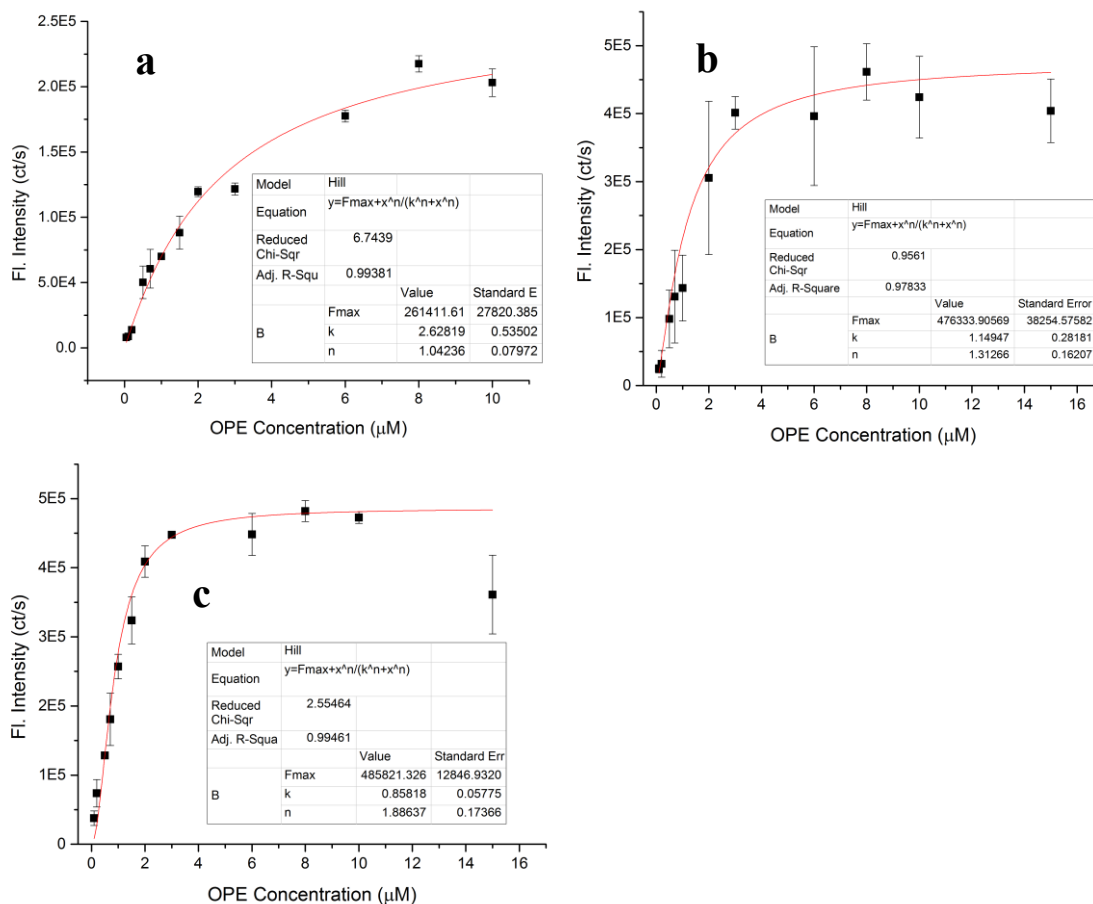
Figure III.9. Saturation binding assay curves for OPE1+ (a), OPE2+ (b), and OPE3+ (c). Protein concentration (9h aggregates): 5 µM monomer basis / 0.25 mg/mL. Fits to the Hill equation were carried out in OriginPro 9 without constraining any parameters. Experiments were performed in duplicates and error bars represent standard deviations.
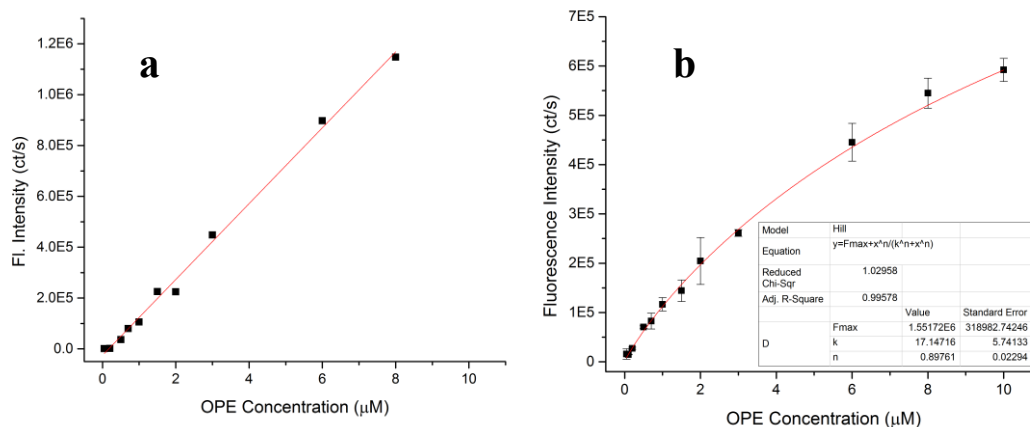
Figure III.10. a: Linear (non-saturable) binding of OPE1- to HEWL monomers (5 μM / 0.25 mg/mL). Linear fit shown for clarity. This experiment was performed once. B: Attempted binding assay of OPE1- to HEWL amyloid, showing effect of non-specific binding to monomers.

Induced Circular Dichroism of OPE-Amyloid Complexes
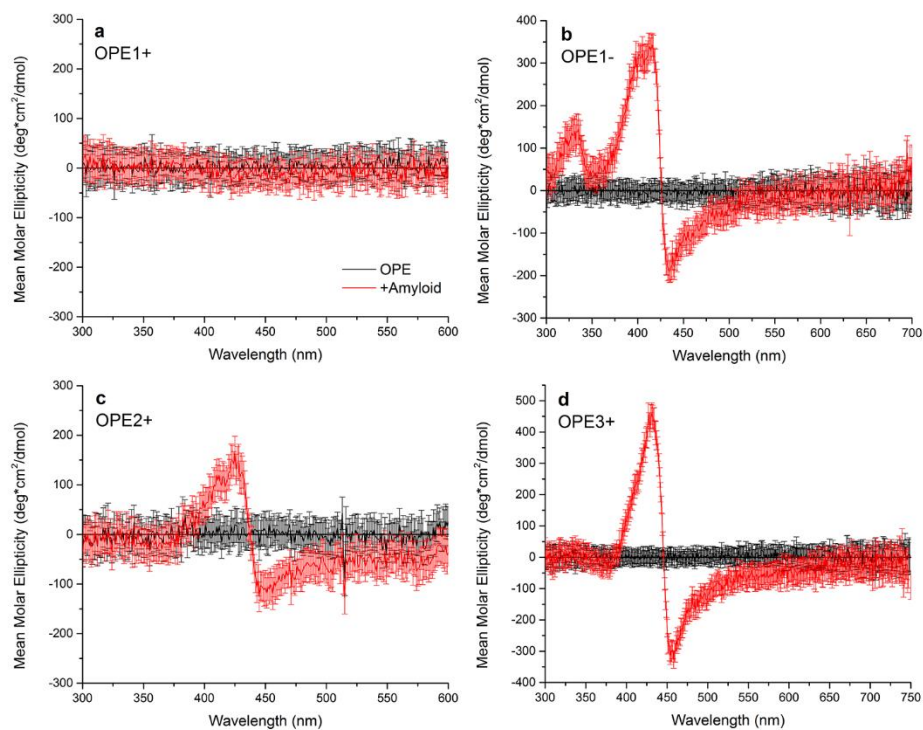
Figure III.11. Circular dichroism spectra of OPEs in PB with HEWL monomer (black trace) and with HEWL amyloid (red trace). (a): OPE1+; (b): OPE1-; (c): OPE2+; (d): OPE3+. OPEs 10 μM, HEWL 10 μM monomer basis / 0.5 mg/mL.

Twists are often observed in mature amyloid fibrils, including HEWL fibrils prepared in this study (Figure III.4d, inset). This twist or other intrinsic chirality of the HEWL molecule might induce chirality in bound ligands. To test this hypothesis and gain further insights into the structure of bound OPE states, CD measurements were taken in the OPE absorbance range to determine if the intrinsic chirality of the HEWL fibrils was transferred to the OPE chromophore by a chiral backbone twist or an "excitonic" chiral supramolecular aggregate. CD spectra (Figure III.11) indicated that OPEs became optically active when bound to HEWL amyloids, as shown in Figure III.11. As expected, no OPE had optical activity by itself in phosphate buffer solution and non-binding cationic OPEs were not optically active with HEWL monomers. OPE1-, which did appear to bind to monomers, though somewhat weakly, also had no optical activity. OPE1+ did not have optical activity with HEWL amyloid, but the other three OPEs did. OPE1-, OPE2+ and OPE3+ all had strong induced CD with a negative Cotton effect when bound to HEWL amyloid fibrils. OPE2+ and OPE3+ gave rise to similar CD spectra, with more intense bands in the spectrum for OPE3+. The induced CD spectrum for OPE1- had a pronounced two-band structure, reflecting the more intense high-energy band for the anionic OPE when bound to HEWL amyloid.

Protein→OPE Energy Transfer in OPE-Amyloid Complexes
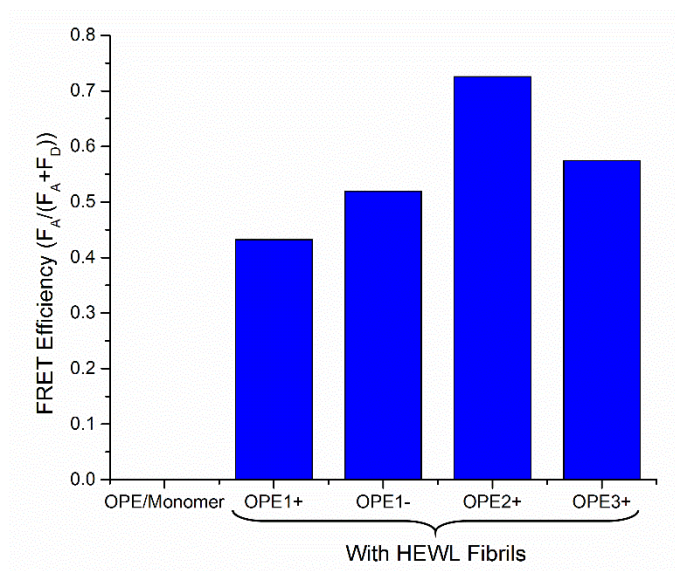
Figure III.12. HEWL→OPE FRET efficiencies calculated from spectral data (Supporting Information) by Equation 1. Data from control experiments can be found in Supporting Information.
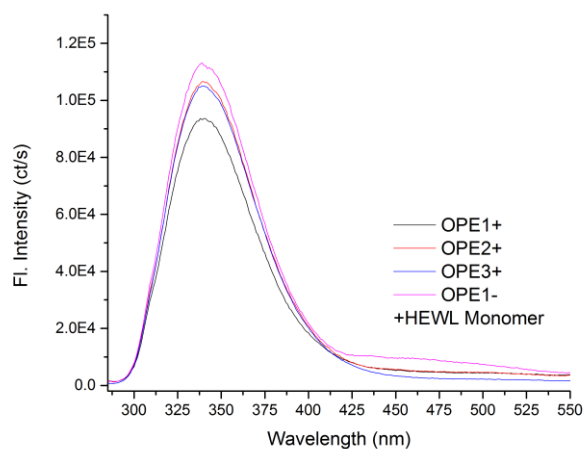
Figure III.13. Fluorescence spectra of OPEs mixed with HEWL monomers showing a lack of energy transfer from HEWL monomer to OPE as no OPE fluorescence in the 400-550 nm range was observed.
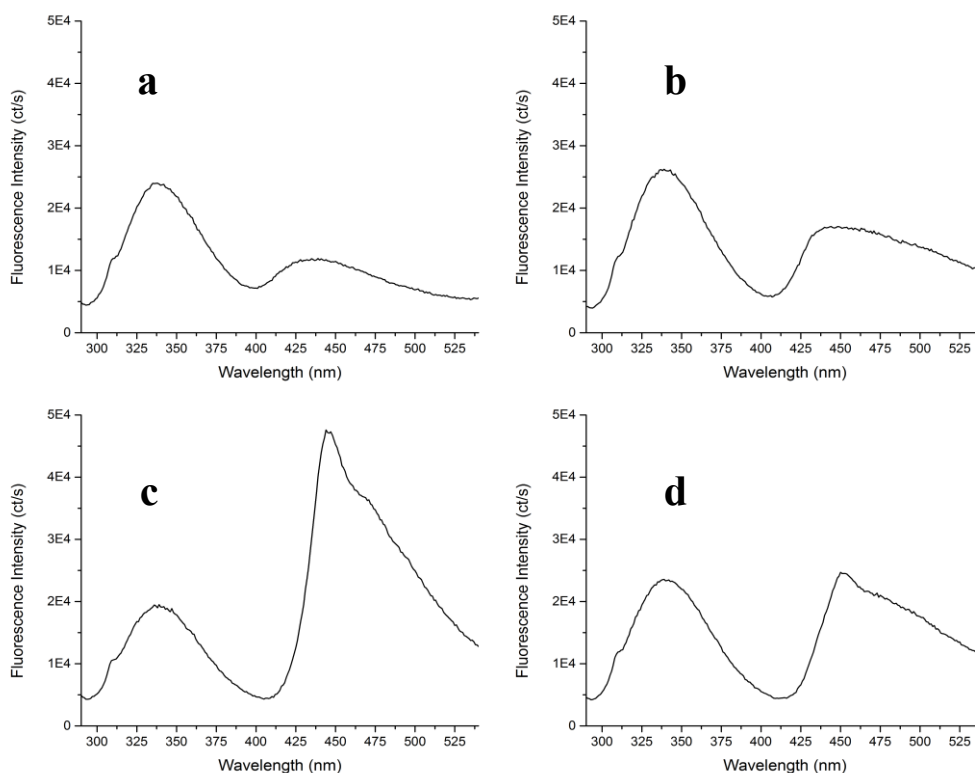
Figure III.14. Emission spectra of OPEs (a: OPE1+, b: OPE1-, c: OPE2+, d: OPE3+) (500 nM) in PB with HEWL amyloid (9h aggregates, 5 µM monomer basis / 0.25 mg/mL) excited at 280 nm. Low wavelength peak (300-375 nm) is lysozyme native fluorescence and the high wavelength peak (400-550nm) is OPE fluorescence.

Since lysozyme is an intrinsically fluorescent protein whose emission spectrum in the 320-380 nm wavelength range overlaps significantly with the excitation spectra of OPEs (Figure III.13), we investigated the possibility of Förster resonance energy transfer (FRET) from the protein chromophore to OPEs by a simple spectroscopic method. Emission spectra of solutions containing OPEs and HEWL amyloids or monomers were obtained using the excitation wavelength of HEWL (280 nm) and OPE emission was observed only from OPE/amyloid samples, indicating that HEWL→OPE energy transfer was occurring only with OPEs bound to amyloid fibrils. The results are summarized as FRET efficiencies (E) in Figure III.12. The raw spectral data (Figure III.14) was converted to efficiencies by the equation

$$E = \frac{F_A}{F_D + F_A} \text{ (Equation 2)}$$

where F_D is the integrated area under the donor emission peak, and F_A is the integrated area under

the acceptor emission peak. This simple expression is valid for this case since the OPEs are

nonfluorescent when excited at the donor excitation wavelength of 280 nm, eliminating crosstalk.

Thus, F_A is the total number of energy transfer events, and (F_A+F_D) is the total number of

excitation events. Theoretically, the efficiencies should be convertible into distances by

$$E = \frac{1}{1+(\frac{r}{R_0})^6}, \text{(Equation 3)}$$

However, because OPEs and HEWL amyloids are not a well-characterized FRET pair with a

defined Förster radius R_0, and calclulating R_0 for a protein-ligand pair not freely rotating relative

to each other in solution is rife with inaccuracies[2], we cannot directly evaluate distances in the

OPE-HEWL system. Qualitiatively, we can make some determinations based on the relative

measured efficiencies for the different OPEs. The measured FRET efficiency will be affected by

multiple independent factors averaged over all the OPE-HEWL pairs in solution, such as the

number of bound OPE molecules, the bound OPE-HEWL chromophore distance, and the spectral

overlap integral $J(\lambda)$, all of which will vary by OPE. The highest apparent efficiency observed for

OPE2+ is probably the result of its higher binding constant than OPE1- or OPE1+ combined with

its greater overlap integral than OPE3+.
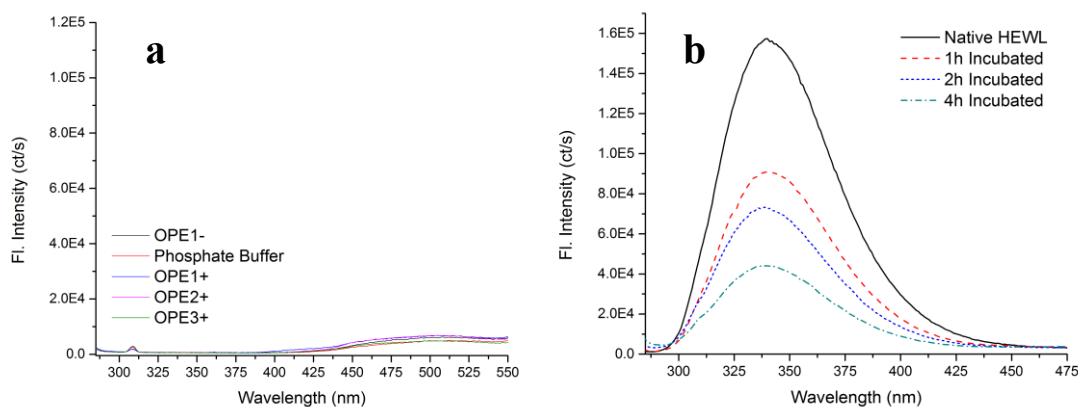
Figure III.15. a: Control experiments showing that OPEs alone are non-fluorescent when excited at 280 nm. B: Emission spectra of 0h (black solid line), 1h (red long dashed line), 2h (blue short dashed line) and 4h (green dot-dashed line) incubated HEWL, λ_{ex}=280nm, showing reduction in intrinsic protein fluorescence over the process of amyloid formation.

Explicating the Mode of OPE-Amyloid Binding
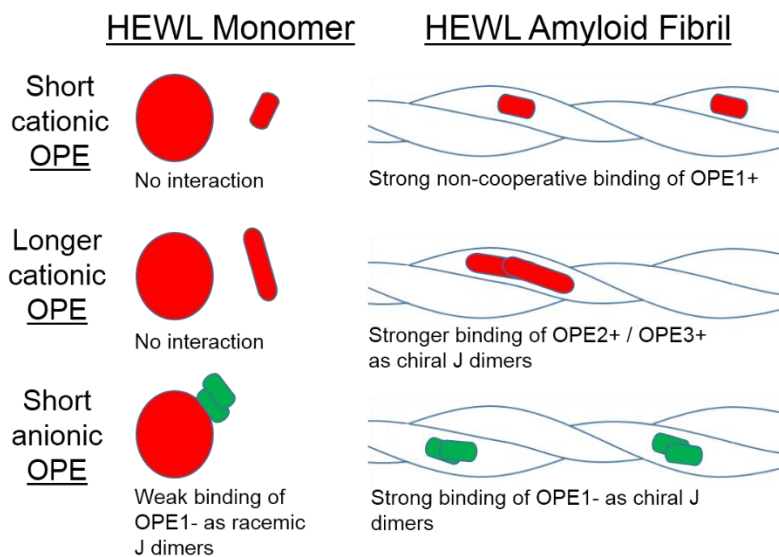
Figure III.16. Illustration of proposed binding modes of OPEs to HEWL monomers and amyloid fibrils.

The results of these experiments led us to hypothesize modes of interaction between

OPEs and HEWL monomers and amyloids, as illustrated in Figure III.16. All four OPEs tested

were observed to bind to HEWL amyloid, with good affinity, but with different properties

depending on chain length and charge. Generally, the OPEs either do not interact with protein, bind as single molecules, or bind as J dimers which are either racemic or chirally biased. The changes in the excitation spectra of OPE2+ and OPE3+ when bound to amyloid are also highly reminiscent of the absorbance spectra observed for the same compounds when complexed with carboxymethylcellulose[45]. Overall, it has become clear that J-type aggregation is a naturally favorable mode of OPE-OPE interaction for OPEs with charged side chains when the Coulombic repulsion between the charged groups is reduced.

The spectral changes of OPE2+, OPE3+, and OPE1- in complex with HEWL amyloids, and of OPE1- in complex with HEWL monomers, are highly indicative of J aggregation: redshifted absorbance, sharpening of fluorescence band, and narrowed Stokes shift. The enhancement of fluorescence intensity is attributable all or in part to the reduced quenching of the OPE by water when bound to the hydrophobic sites on the surface of the protein; this solvent-access effect is in play for all four OPEs. The current study indicates that the longer cationic OPEs, OPE2+ and OPE3+, form J dimers (or possibly larger aggregates) on the HEWL amyloid fibril surface, and OPE1- forms J dimers on both HEWL monomers and HEWL amyloid fibrils. The OPE aggregates formed on amyloid fibrils have a chiral bias to the OPE-OPE offset angle, producing a chiral supramolecular chromophore, or an excitonic optical activity, responsible for the circular dichroism seen experimentally (Figure III.11). The exact source of this bias is hard to pin down; it could be a result of the helically twisted fibril axis (see Figure III.4d, inset) or more specific to a binding site. Notably, the aggregates formed by OPE1- must be racemic, indicating that the OPEs are not interacting with a specific site but simply binding to oppositely charged residues on the lysozyme surface. OPE1+ exhibited some small redshifts in the excitation spectrum, but its emission spectrum does not shift at all and it acquires no optical activity, indicating that this compound binds to HEWL fibrils as single molecules rather than as a structured aggregate. The small excitation redshift could be due to minor backbone planarization, and the increase of fluorescence intensity to reduced solvent access.

The results of binding saturation assays support these conclusions for the cationic OPEs. OPE2+ and OPE3+ show positive cooperativity, meaning that the binding of one OPE increases the affinity of the next binding event. The formation of J aggregates on the fibril surface satisfies this condition: a single OPE might bind to a favorable site, and a second finds it and forms an even more favorable J aggregate due to π-π and hydrophobic interactions. It is also possible that OPEs could form J dimers in solution that subsequently find the fibril surface, but this seems unlikely due to charge repulsion. Furthermore, the binding curve for OPE3+ shows a larger cooperative effect than that for OPE2+, and the induced CD bands for OPE3+ are also more intense; the increased length of OPE3+ increases the available area for aggregate formation, forming more or larger chiral aggregates. The OPE1+/HEWL amyloid binding assay indicated no cooperative binding effect, which is consistent with independent, single-molecule binding. The decrease of apparent dissociation constant K with increasing OPE length is in agreement with the results of previous studies indicating that longer linear conjugated regions increase affinity for a long hydrophobic binding site on amyloid[27].

One notable result of this study is the large differences between OPE1+ and OPE1- in their interactions with HEWL monomers and amyloid, as shown in Figure III.16. These two single-repeat OPEs tested differ only by the charge on the side-pendant solubilizing groups (Figure III.1), and their interactions with HEWL monomer and amyloids were highly different. OPE1+ exhibited non-cooperative and saturable binding to amyloid fibrils without induced optical activity or large shifts in absorption or emission bands, and when bound, its emission was the least enhanced over free OPE. Its anionic counterpart, OPE1-, proved quite different both in its nonspecific binding to HEWL monomer and in its interaction with HEWL amyloid. The interaction of OPE1- with HEWL monomers has been noted in an analogous system, with sulfonate-bearing p-phenyleneenthynylene polymers[64], and is mediated by hydrophobic and electrostatic interactions with the positively charged (at neutral pH) lysozyme. This interaction was seen to be fairly weak and non-specific, as indicated by the non-saturable binding, but it

overwhelms the OPE1-/amyloid interaction at high OPE concentrations, after all the amyloid binding sites are occupied. *In vitro*, without interfering effects from other cellular/tissue components, such an effect could prove useful for monitoring the disappearance of similarly charged monomers. The differences in the OPE1+ and OPE1- binding to amyloid—OPE1+ binds singly and OPE1- as chiral J aggregates—could be due to charge or H-bonding interactions specific to sites on the lysozyme fibril surface. The specificity of these possible charge effects is notable, since the arrangement of charged residues on the fibril surface is controlled by the protein's primary, secondary and tertiary structures. This effect could provide useful means of differentiating amyloids formed from different monomers.

Analysis of the energy transfer from HEWL amyloids to OPEs corroborates many of these proposed binding modes. The absence of FRET in any monomer/OPE solution reconfirms the weak and non-specific nature of OPE1-/monomer binding, since the OPE is not held within range of the fluorescing aromatic residues. In natively folded conformations of globular proteins such as lysozyme, hydrophobic residues are typically buried in the hydrophobic interior of the protein and not solvent, or ligand, accessible. Aromatic residues may also only be surface exposed, available for binding, and within range of FRET to OPEs in the amyloid state; HEWL intrinsic fluorescence is found to decrease over the course of incubation (Figure III.15b), which implies that the fluorescing residues are increasingly exposed to solvent quenching as more amyloid forms. The very strong distance dependence of FRET effects (typically <10nm)[2,65] provides a strong constraint on the possible location of OPE fluorophores on the fibril surface. When combined with computational simulations, this FRET effect could shed some light on the molecular structure of other, more closely disease-related amyloid-forming proteins with intrinsic fluorescence.

Our results, especially the effects of ligand charge, are clearly influenced by the primary sequence of the protein monomer used to form amyloid. Performing future work with disease-related amyloid proteins and peptides, and ideally with sections of actual diseased tissue or in

well-characterized animal models, is critical to developing OPEs, or other molecules, into viable tools for researchers and, eventually, clinicians. The large differences between OPE1+ and OPE1-'s interactions with monomeric and amyloid HEWL, likely influenced by specific charged residues in the HEWL primary sequence, seem promising for differentiating amyloids formed from different protein monomers, a useful effect, for example, in the study of dementia with Lewy bodies[66], in which Lewy bodies (formed of the protein alpha-synuclein and normally characteristic of Parkinson's disease) and amyloid plaques are comorbid.

IV. Broader Testing of OPE/PPE Library with Two Model Amyloids

1. Background

After testing a small subgroup of OPEs as amyloid detection agents, found them to be effective, and developed some hypotheses as to the molecular mechanisms underlying their effectiveness, the next step was to challenge our assumptions by testing a larger library of OPEs and PPEs using more model amyloids. The previous project had focused only on ethyl ester-bearing OPEs, but the necessity of this moiety for sensor function had not been determined. The "steric targeting" property had also to be determined empirically by testing the pre-existing ligand library against various types of amyloids. Furthermore, the model amyloid system had to be expanded to include another type of protein monomer.

2. Methods

Except OPEs, all reagents were obtained commercially and used without further purification. Synthesis of OPEs has been reported previously[45], except for OPE1-, which was synthesized analogously to OPE1+. Hen egg white lysozyme, bovine insulin and Thioflavin T were obtained from Sigma-Aldrich Chemical Company (St. Louis, MO). Suspensions of protein aggregates were gently vortexed to distribute aggregates before use in experiments.

To make amyloids, HEWL was dissolved at 5.46 mg/mL in an acidic buffer (10 mM sodium citrate, pH 3, 0.1 M NaCl) and incubated at 70°C for 12h with 250 rpm magnetic stirring. For insulin fibrils, a 10 mL stock solution of insulin was prepared at 10 mg/mL in pH 3 citrate buffer, with a drop of HCl added to solubilize the protein, and the stock was diluted to 5.46 mg/mL and incubated under the same conditions as HEWL. Extinction coefficients at 280 nm of 1.0 L/g*cm for insulin[67] and 2.63 L/g*cm for lysozyme[68] were used to determine concentrations.

Both protein solutions, initially clear, formed a cloudy precipitate within an hour of heating. For thioflavin T assay, protein and ThT stock were mixed in PB to a final concentration of 5 ug/mL protein and 20 uM ThT and emission spectra obtained with 440nm excitation and 480nm emission.

For AFM, a droplet of each protein sample at 5 mg/mL was pipetted onto freshly cleaved mica substrate and allowed to physisorb for 20 mins, followed by a single rinse with HPLC-grade water and gentle drying under a stream of N_2. Imaging was performed with a Nanoscope IIIa AFM (Veeco, Plainview, NY) or Asylum Research MFP-3D-BIO in tapping mode under a constant stream of dry N_2 gas using a rectangular silicon cantilever with a spring constant of 40 N/m (Veeco model RTESPA-W).

Spectroscopic assays were conducted as follows. In the wells of a 96-well plate, monomeric protein, amyloid or a buffer blank was diluted with CPE stocks into 10 mM pH 7.4 phosphate buffer to a final concentration of 2 uM OPE or 1.88 ug/mL PPE (same monomer concentration as the intermediate-size OPEs) and 5 ug/mL protein. The plates were then read on a plate-reading spectrophotometer (SpectraMax M2e, Molecular Devices, Sunnyvale, CA) for absorption and emission spectra. Final sample volume was 200 uL, and each well was prepared in duplicate. For more detailed evaluation of spectral changes, a steady-state cuvette-reading fluorimeter (PTI QuantaMaster 40, HORIBA Scientific, Edison, NJ) was used. The same concentration and sample volumes were prepared and transferred to a small-volume quartz fluorimetry cuvette (Starna Cells, Atascadero, CA), and excitation and emission spectra were obtained.

For protein intrinsic circular dichroism, protein samples were diluted in sodium citrate buffer without NaCl (pH 3, 10 mM) to a concentration of 0.14 mg/mL, vortexed briefly, and read in a quartz CD cuvette (1mm pathlength) using an Aviv 410 CD spectrometer (Aviv Biomedical, Lakewood, NJ) with a 15s averaging time. A blank spectrum (buffer only) was subtracted from each sample to remove background signal. Error bars are standard deviation over multiple reads

of a single sample as reported by the AVIV software. For OPE induced circular dichroism, OPEs and protein were diluted in phosphate buffer (pH 7.4, 10 mM) to an OPE and protein concentration of 5 μM, and data was obtained and processed identically to the protein CD experiments. OPEs and protein samples were diluted in phosphate buffer, gently vortexed, and read in a 1mm pathlength quartz CD cuvette using an Aviv 410 CD spectrometer (Aviv Biomedical, Lakewood, NJ), 15s averaging time. A blank spectrum (PB only) was subtracted from each sample to remove background activity. Error bars are standard deviation over multiple reads of a single sample as reported by the instrument.

For binding constant determinations, matured fibrils were first separated from residual monomeric and smaller aggregated proteins by repeatedly passing diluted solutions through Amicon centrifugal filter units (EMD Millipore, Billerica, MA) having a 30 kDa molecular weight cutoff. The concentration of the resulting fibril concentrates was determined by absorbometry at 280 nm. OPE/fibril solutions were prepared with 500 nM protein concentration and a range of OPE concentrations, read on the spectrofluorometer, the peak fluorescence plotted against ligand concentration and the curve fit to the Hill equation in OriginPro 9 without constraining any parameters.

3. Discussion

This project evaluated the binding-activated photophysical changes to the members of a library of poly- and oligo(phenylene ethynylene) electrolytes upon interaction with lysozyme and insulin model amyloids. The compounds in the screening set are detailed in Table IV.1. This set comprised 18 different phenylene ethynylenes, thiophene ethynylenes, and one phenylene ethynylene-thiophene ethynylene copolymer, with solubilizing cationic and anionic groups attached on the sides or ends of the backbone. The compounds bearing ethyl ester substituents were predicted to exhibit much better sensing activity due to their possession of a solvation-

triggered nonradiative decay pathway, but we chose to evaluate all the compounds to test for

possible alternate binding-triggered mechanisms such as molecular-rotor behavior.[28,69]

Backbone	Substituents			Cmpd.
	Ar = (phenyl)	R = (trimethylammonium, Br⁻)		A1
	Ar = (thiophene)	R = (trimethylammonium, Br⁻)		A2
	Ar = (phenyl)	R = (bicyclic diammonium, 2Br⁻, C₆H₁₃)		A3
	R = (trimethylammonium, Br⁻)	R' = H	n = 1	B1
			n = 2	B2
			n = 3	B3
		R' = (ester, OEt)	n = 1	B4
			n = 2	OPE2
			n = 3	B5
	R = (sulfonate, Na⁺)	R' = H	n = 1	B6
		R' = (carboxylic acid, OH)		B7
		R' = (ester, OEt)		OPE1
	R = (sulfonate, Na⁺)		n > 1000	C1
	R = (bicyclic diammonium, 2Br⁻, C₆H₁₃)			C2
	R = (methylimidazolium)			C3
	R = (methylimidazolium)			C4
	R = (trimethylammonium, Br⁻)			C5
	R = (methylimidazolium)			C6

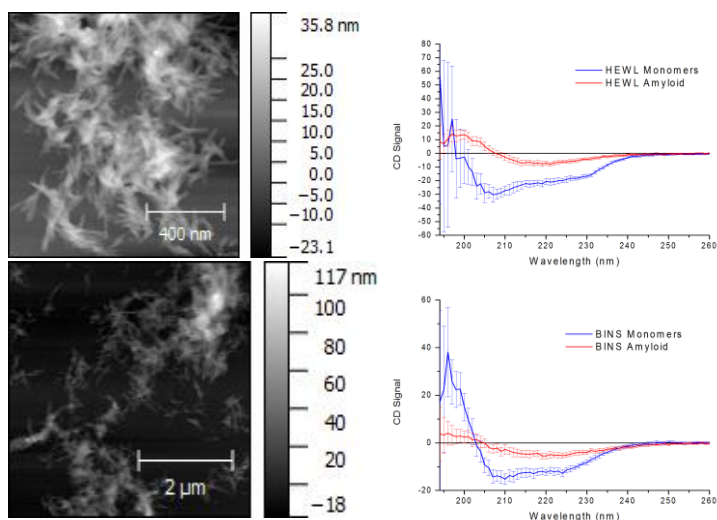Table IV.1. Table of compounds tested against model amyloids.

Figure IV.2. AFM and circular dichroism of protein preparations confirming the presence of linear, beta-sheet enriched aggregates. Top: lysozyme; bottom: insulin.

Preparation of model amyloids was performed using literature procedures.[70,71] Lysozyme and insulin were chosen for their well-studied amyloid-forming properties and differing charge distributions at neutral pH, and amyloids were formed simply by heating the protein in acid. Amyloids were prepared by incubation of protein solutions at 70°C and a buffered pH of 3. Far-UV circular dichroism spectroscopy (Figure III.2) indicated transformation of the primarily alpha-helical native secondary structures of both proteins into the beta-sheet structure indicative of amyloids. Atomic force microscopy of incubated protein solutions deposited on mica (Figure III.2) revealed that both proteins formed bundled, short fibrillar aggregates, with individual linear structures about 100 nm long and 20 nm wide, composed of two or more twisted sub-fibrils. These amyloid aggregates also tested positive using the gold-standard thioflavin T binding assay. Taken together, under high heat and acidic conditions, both model amyloid proteins readily formed fibrillar, beta-sheet enriched aggregates that are thioflavin-T positive.

Testing of candidate dyes against model amyloids was performed by spectrophotometry of dilute solutions of dye alone, dye with monomeric protein, and dye with aggregated protein. After taking emission spectra of each candidate dye in buffered solution, with monomeric protein and with amyloid fibrils, we defined a dimensionless quantity Q as described in Equation 1:

$$Q = \frac{F_{+fibril} - F_{+monomer}}{F_{buffer}} \quad \text{(Equation 1)}$$

Where $F_{+fibril}$, $F_{+monomer}$ or F_{buffer} indicates the integrated emission intensity for the dye

under the relevant condition. Figure III.3 summarizes the Q values measured for each dye in the

screening set. Values of Q close to zero indicate that the dye failed to differentiate between

fibrillar and monomeric protein, negative values indicate that the dye interacted strongly with

monomeric protein, and positive values indicate that the dye selectively detected amyloid

conformations.
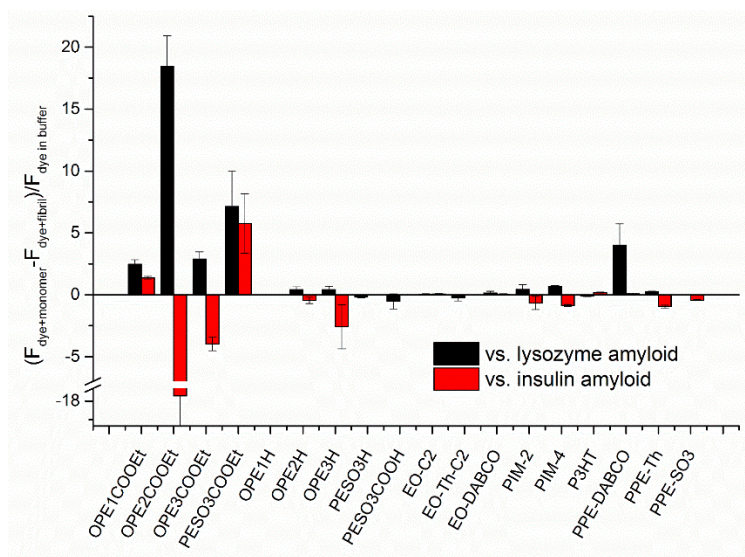
Figure IV.3. Chart of detection response values, calculated from fluorescence data using Equation 1 for each dye in the screening set. Error bars are SEM.

The values shown in Figure III.3 indicate that the COOEt-terminated compounds gave

the greatest changes in fluorescence yield upon interaction with protein, and moreover that the

only compound with effective sensor response to amyloid (defined as positive Q for both

lysozyme and insulin amyloid *i.e.* specificity for the amyloid conformer over monomeric protein)

was OPE1.

Despite the large solvent-sensitive emission yield and favorable morphology of the H-

substituted dyes, their performance as amyloid-detecting ligands was poor. Binding to amyloid, if

it occurs, fails to stabilize a planar configuration of the backbone in singly bound dye, resulting in

a dark bound state. By contrast, the ester-substituted dyes are sterically shielded from solvent access in the bound state, resulting in significantly increased fluorescence upon binding. Disentangling rotational internal conversion from self-quenching by aggregates from solvent-mediated quenching is exceptionally difficult in systems of amphiphilic dyes, but substantial circumstantial evidence favors the interpretation that fluorescence of phenylester OPEs is suppressed in water by a mechanism that is not intramolecular rotational internal conversion, not least of which being that computational results show planar lowest-energy ground and excited states.[72] Additionally, if quenching process in the COOEt molecules is rotationally based, then we would expect to see increased fluorescence yield in water, with the increased solvent-ester H-bonding interactions increasing drag on the rotation of the terminal phenyl ether.[73]
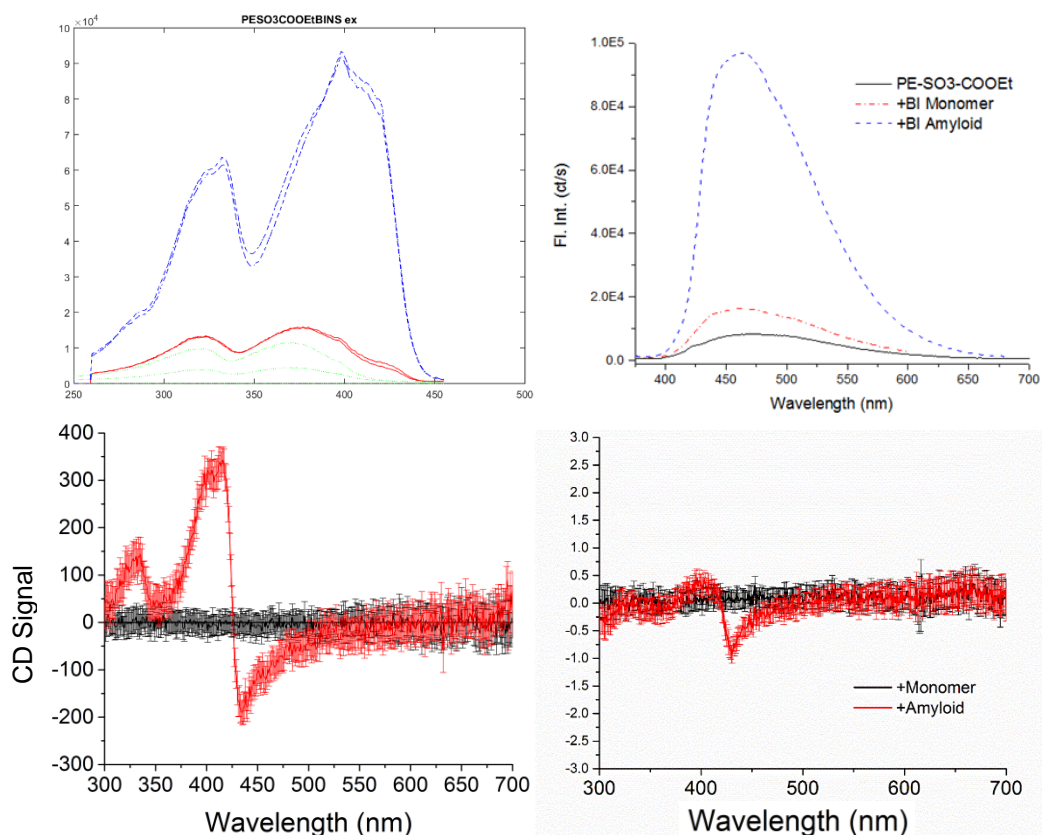
Figure IV.4. Fluorescence excitation and emission spectra (top) and circular dichroism spectra (bottom) of OPE1 in buffer solution and bound to amyloids.

Contrary to our expectations, polymeric dyes did not perform effectively as dyes for any type of amyloid. Despite their great length, our previous observation of positive correlation between molecular length and amyloid binding affinity, and differences in emission yield depending on the state of self-aggregation, the effectiveness of these conjugated polyelectrolytes was low. Possibly chain-chain interactions along the polymer are too strong to be overcome by the binding to amyloid. Even previous groups to have explored polyelectrolyte dyes for amyloid[74] have since moved to small-molecule derivatives for better controllability, effectiveness and in-tissue transport properties. The smallest compounds tested, the linear end-functionalized dyes A1, A2 and A3, were also completely ineffective as amyloid sensors due to their binding to monomeric protein. These compounds, as mentioned above in Project I, have previously been

shown to interact with the membranes of Gram-positive and –negative bacteria and disrupt them. This non-amyloid-specific intercalative mechanism is a significant drawback.

Along with desolvation-triggered dequenching, the second mechanism involved in the fluorogenic performance of OPE1 is the formation of luminescent, protein-templated J-aggregates. J-aggregates have a long history in the chemistry of organic dyes and are defined as aggregates with hypsochromic (red-shifted) absorbance bands, increased fluorescence yield and decreased Stokes shift compared to monomeric dye[57]. The controlled aggregation of phenylene ethynylenes has been exploited before to engineer solution-phase sensor systems, and is a useful way to control analyte-sensitive changes in optical properties. The formation of aggregates in amyloid-templated OPE systems is indicated by J-type changes in spectral properties and the broken symmetry (as indicated by induced circular dichroism) of the amyloid-bound OPE absorption band. In the amyloid-bound OPE1, absorption maxima are observed to redshift and fluorescence band narrows and increases in brightness (due also to the reduction of solvent quenching), indicating the formation of J-type aggregates. Similar spectroscopic changes are observed in surfactant/dye systems, as well as complexes of dyes with carboxymethylcellulose, hypothesized to contain J-aggregates.[45,56] OPE1 also develops induced circular dichroism when bound to amyloid, which could be due to chiral backbone twisting but is more likely due to the formation of stacked J-aggregates in short chiral helices. If chiral backbone twisting was responsible for the strong induced CD signal, the reduction in mean chromophore length would appear as a significant blueshifted band, which is not observed.

4. Conclusions

The results of this project show that oligo(*p*-phenyleneethynylene) electrolytes are an effective molecular scaffold for selective sensing of the amyloid fibril conformer of the model protein HEWL. OPEs exhibit drastic fluorescence enhancement and useful absorbance redshift when introduced to the HEWL amyloid conformer, and binding constants were determined to be

usefully low, ~1 μM. Furthermore, the amyloid-sensing properties—fluorescence enhancement, cooperative binding and induced optical activity—are hypothesized to be due to the propensity of the dye molecules to form chiral, superluminescent J aggregates templated on the amyloid fibril surface. Although the OPEs used in this study were not designed or optimized for amyloid binding, they still performed effectively compared to Thioflavin T, the amyloid dye currently in widest use. The fluorescence properties and optical activity of the bound OPEs are highly dependent on OPE chain length and charge. The longer, cationic OPEs are the most promising ligands for imaging purposes among the molecules tested in this study. OPE2+ and OPE2+, in particular, have low enough apparent binding constants and optical bandgap to possibly be used immediately for *ex vivo* staining. On a molecular level, several effects are probably at work, including restriction of internal rotation, planarization, reduction of quenching by water and J-type aggregation. For all four OPEs, reduction of quenching by water when bound to the hydrophobic site is responsible for some of the drastic fluorescence enhancement.

IV. Sensing in a Tissue Environment: Sensing of Amyloids II

1. Background

Having established the efficacy *in vitro* of small linear phenyleneethynylene electrolytes in both selectively binding to amyloid conformers and undergoing a desolvation-triggered increase in fluorescent yield, a logical next step was to evaluate their extensibility to the much more complex and crowded environment of fixed animal tissue. Formalin-fixed brain sections present many sites of competitive binding and places for the dye to "get stuck," and performance and selectivity in this environment is a crucial test.

2. Methods

Tissue sections were prepared with the help of Dr. Kiran Bhaskar and Nicole Maphis at the MIND Institute at UNM Health Sciences Center. Tissue used was from 9-month-old rTg4510 human tau-expressing mice, two-month-old B6 wild-type laboratory mice, or 20-month-old R1.40 mice expressing human amyloid precursor protein with Swedish mutation and human presenilin with familial mutation.[75] Tissue was already sectioned at the time of experiment and stored in cryoprotectant solution. Previous to our experiments, mice were anaesthetized, sacrificed with CO and transcardially perfused with phosphate buffered saline. After dissection, whole brains were fixed with 1% paraformaldehyde, flash-frozen in cryoprotectant solution and sectioned at a width of 30 microns using an ultramicrotome. Sections were stored in liquid glycerol at $0^{\circ}C$ before use. For staining with OPE1 and OPE2, sections were brought to room temperature, washed twice for 15 minutes in PBS and immersed in a 5 uM aqueous solution of dye for 1 hour, then washed twice more in buffer. Sections were laid on glass slides, covered with hardset antifade medium and a coverslip mounted. Imaging was performed on a Leica SP8

inverted laser scanning confocal microscope with 405nm laser diode illumination for OPE and other dye lines as indicated in individual figures.
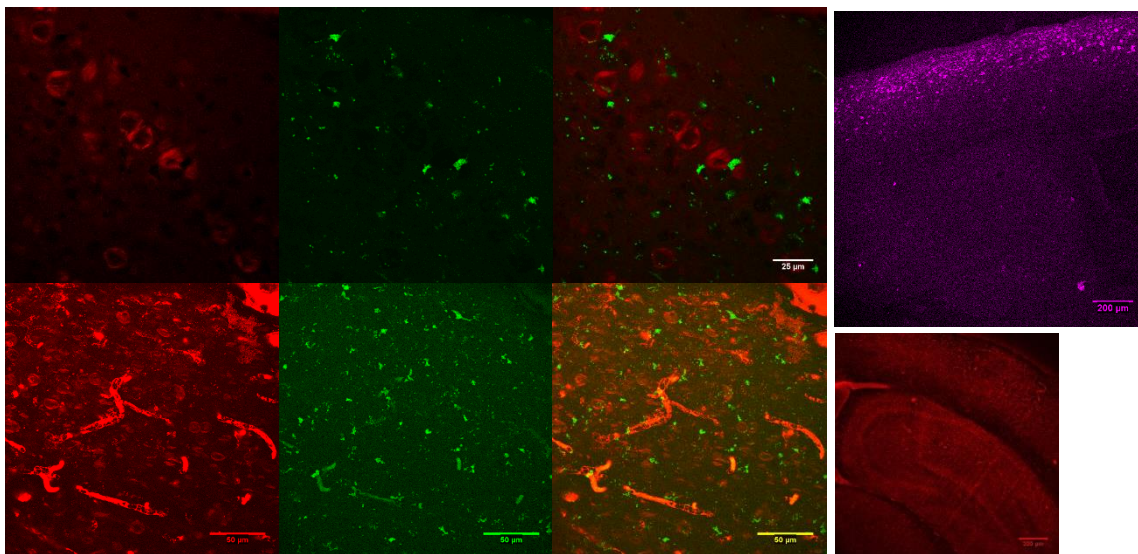
3. Discussion

Figure IV.1. Staining of rTg4510 tau-expressing mouse brain sections by OPE1 (top) and OPE2 (bottom). Green channels are autofluorescence from lipofuscin granules. Ring-shaped neurofibrillary tangles are visible throughout the cortex. In the OPE2 images sections of vasculature are also stained, for unknown reason.

After determination of the best-performing compounds from the selective screening assay, they were evaluated for performance in ex vivo tissue staining, using a human tau-expressing transgenic model mouse.[76] 30 um thickness sagittal sections of whole paraformaldehyde-fixed brains of rTg4510 neurofibrillary tangle-positive mice were immersed for 30 minutes in a 5 um solution of dye and washed twice in PBS to remove excess dye. The results, for OPE1 and OPE2, mirror the results of the in vitro assay and confirm the soundness of the screening methodology. Even before optimization, the lead candidate OPE1 performs as well as ThT in tissue staining, with low background, no undesired binding and bright emission. OPE2, by contrast, found to be less selective in vitro, proves to have significant binding to an unknown factor in the vasculature of both transgenic and wild-type mice. Results of these staining

experiments deliver parallel results to those in the *in vitro* screening study: OPE1 proved selective for the amyloid conformer, while OPE2 bound undesirably to some monomeric protein.

OPE1 staining was also effective in R1.40 APP/PSN1 transgenic mice expressing amyloid plaques and in human brain tissue from patients with tau-associated frontotemporal dementia. The effectiveness of OPE1 was also evaluated against paired helical filaments of tau purified from human and mouse brain tissue, and against in vitro formed fibrils of ab40 and ab42. Interestingly, spectral imaging of the neurofibrillary tangles and beta-amyloid plaques in brain tissue reveals an emission spectrum of OPE1 that recapitulates that of the free dye, as opposed to that of the dye bound to fibril suspensions in vitro. It is not especially surprising that the binding mode of the dye would change in the crowded molecular environment of the cell.
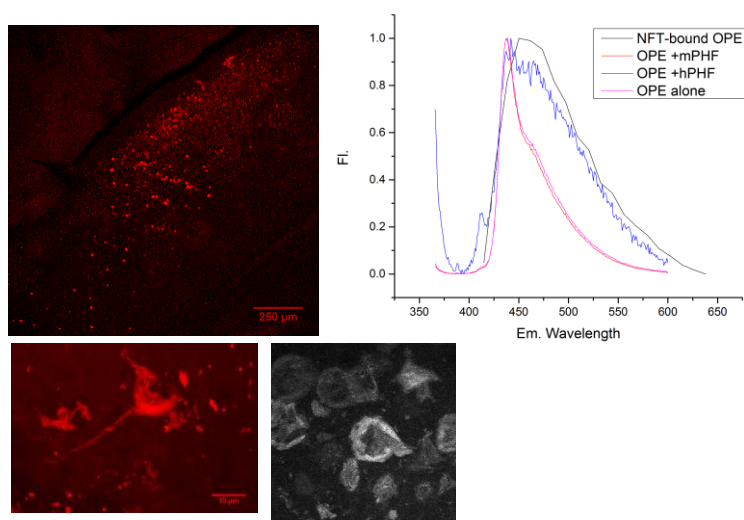

Figure IV.2. Confocal fluorescence images of OPE1 staining amyloid deposits of different kinds, and spectra from ROIs in those images and in vitro cuvette spectroscopy. Anticlockwise from top: R1.40 cortical beta-amyloid plaques, a single neurofibrillary tangle in human frontotemporal dementia sample, cortical neurofibrillary tangles from rTg4510 mouse brain.
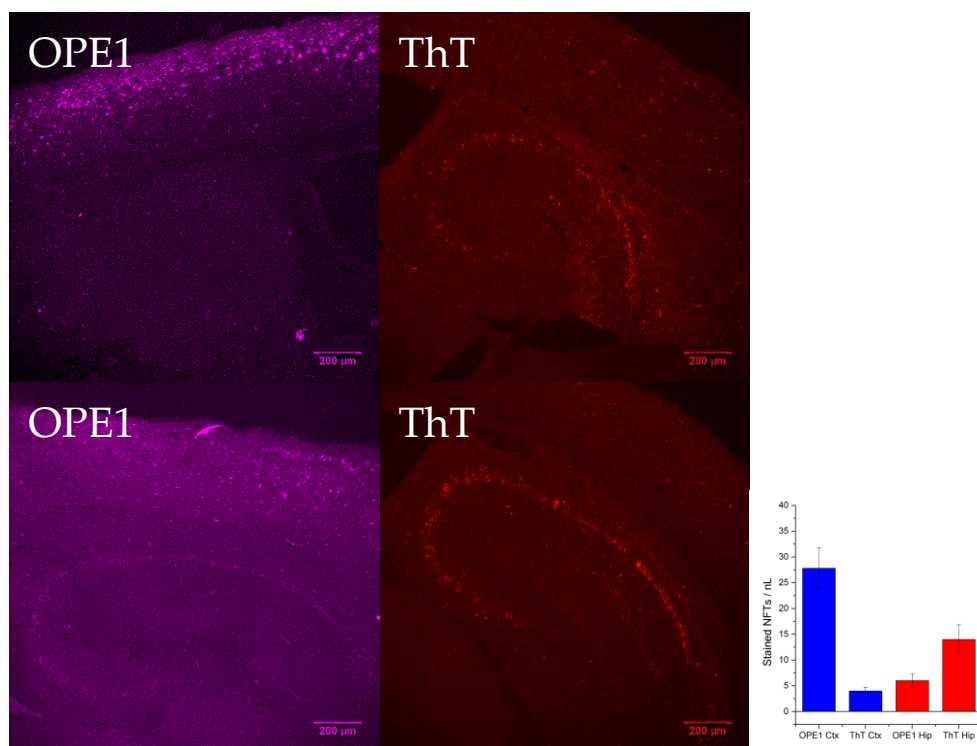
Figure IV.3. Differences in patterns of staining between OPE1 and ThT over the hippocampal-cortical region. Chart reports frequency of tangles per nanoliter in confocal volumes from cortical (Ctx) and hippocampal (Hip) regions stained by OPE1 or ThT.

We also compared the staining patterns of OPE1 and thioflavin T over the whole sagittal sections of Tg4510 mouse brains, and found that while staining is identical at the level of individual tangle morphology, the pattern over different anatomical regions is quite different. Whereas thioflavin densely stains neuronal tau aggregates in the hippocampus, but labels only sparsely in the cortex, OPE1 has the reverse pattern: dense staining in the cortex but sparse in the hippocampus. The precise reason for this difference is unclear, but it presents an intriguing use for OPE1 as a partner to ThT for revealing the complete picture of overall abnormal tau aggregation across tissue.

Of the two dyes tested, OPE1 proved the more effective in terms of practical amyloid imaging. OPE2 was found to bind extensively to an unidentified factor in the vasculature of the amyloid-positive brains, possibly due to the presence of amyloid angiopathy. OPE1, by contrast, bound quite selectively to tau tangles in the cortical and hippocampal regions of Tg4510 mouse

brains, and to amyloid plaques in R1.40 brains, while displaying no binding in wild-type brains. The structures bound by OPE1, and the non-vascular structures bound by OPE2, are similar in morphology and distribution to those found by thioflavin T staining and immunofluorescence with AT8 and AT180 antibodies, though complete colocalization was not demonstrated.

4. Conclusions

These experiments conclusively show the promise of OPEs as a scaffold for amyloid-binding dye development in a tissue environment. OPE1 stains both tau neurofibrillary tangles and beta-amyloid plaques in mouse models, and neurofibrillary tangles in human brain tissue. OPE2 stains the same structures but is hampered by non-selective binding to an additional factor in the vasculature. Emission spectra of OPE1 in tissue are slightly different from those in solution with similar protein aggregates. OPE1 stains similar structures to those stained by thioflavin T but with a different distribution: OPE1 makes cortical tangles more visible, whereas thioflavin T makes hippocampal tangles more visible. The effectiveness of OPE1 is a promising sign for future development of similar compounds.

V. Triplet State Populations Triggered by Solvation/Desolvation

1. Background

Desolvation and assembly into a patterned scaffold can affect more than just the fluorescence of organic dyes. As mentioned in Section II, a useful property of poly(phenylene ethynylene)s and polythiophenes is the good matching of their triplet energy levels with the triplet-singlet transition of molecular oxygen, allowing these compounds to act as Type II photosensitizers.[77] In CH_3OD solution, this process occurs with a quantum efficiency between

0.15 and 0.4 for backbones without heteroatoms and up to 0.64 for thiophene derivatives.[15,78] This photochemical process is catalytic, neglecting photobleaching and self-oxidation, and in practice is a very efficient means of destructively oxidizing cells and viruses to which the dyes will bind. Previous efforts in antimicrobial chemotherapy have focused mainly on controlling migration of the sensitizing dye through exploitation of selective binding as a means to selectively oxidize only target organsisms, and this effect has provided good selectivity for bacterial vs. mammalian cells and membranes.[47,79] However, photosensitizer effects can also be controlled by tuning the underlying photophysical processes. Photosensitization (type II) can only occur if the relevant triplet state is populated sufficiently, and for sufficiently long, to allow an intermolecular collision with free oxygen. The results of projects 1 and 2, as well as previous work by Hill and others, have shown that binding/unbinding of ethyl ester-conjugated dyes can efficiently control fluorescence by swift depopulation (in the solvated, quenched state) of the first excited singlet state. Since the singlet excited state is upstream of all triplet states in the photochemical system under investigation, and the intersystem crossing can be expected to be much slower than radiative decay by fluorescence, the same desolvation-trigger paradigm used to control fluorescence can also be used to control photosensitization and generation of reactive oxygen species.[80]

The approach to this final project was to investigate the viability of controlling triplet state populations by reversible self-assembly of a solvated OPE with surfactants. This possibility was already discussed in an earlier paper by Tang and Ogawa,[78] and could lead to useful applications in controllable photooxidation of a wide range of targets.

2. Methods

Triplet transient absorption (TTA) spectroscopy was chosen as a proxy for singlet oxygen sensitization. Direct observation of singlet oxygen by phosphorescence is limited to specific solvents, and chemical detection introduces too many intervening factors into a delicate balance

of self-assembly. TTA, by measuring directly the intensity and lifetime of triplet-triplet transitions, can provide a great deal of information about the population of triplet states and the rate of their generation and decay.

A solution of OPE1 (2 uM, 0.6 OD at 355nm) was prepared in Millipore water in a 10 mL cuvette with magnetic stirrer and gas-tight septum. The solution was sparged with argon by syringe for 15 minutes before each experiment. TTA readings were performed on a home-built instrument in the laboratory of Kirk Schanze at the University of Florida, using the second harmonic of an Nd:YAG laser (355nm) as a pump source and a broadband flashlamp as a probe source, with a grating monochromator and CCD camera. A stock solution of tetradecyl trimethyl ammonium bromide was added incrementally between readings and the solution sparged again with argon. Delay times were chosen to show the complete decay of the transient peak. Data was analyzed in LabView and MATLAB.
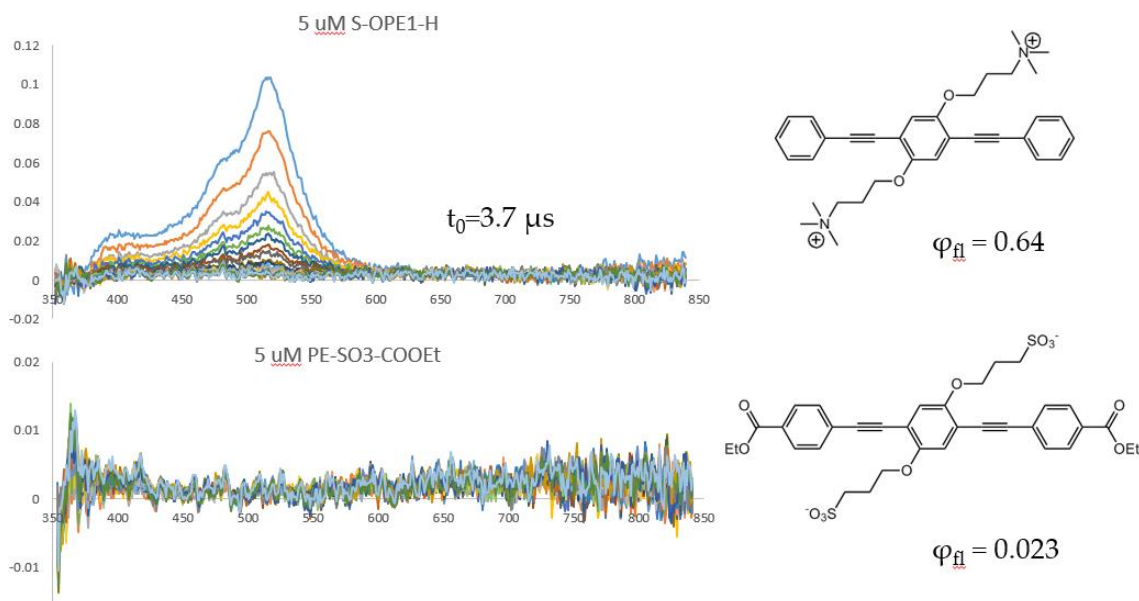
3. Discussion & Conclusions

Figure V.1. TTA traces of S-OPE1-H and OPE1 in H_2O solution, showing the complete lack of a detectable triplet in the ethyl ester-terminated compound. Initial delay: 35 ns; delay increment: 500 ns. Curves shown are the average of 50 images each. Lifetime for S-OPE-1-H was derived by fitting the peak decay curve to first-order kinetics.

TTA traces of OPE1 and S-OPE-1(H) are shown in Figure V.1 above. S-OPE-1(H), which is highly fluorescent in water, exhibits a significant transient absorption peak around 510 nm, decaying with a lifetime of ~4 microseconds. The OPE1, by contrast, has no detectable transient absorption, indicating that either the triplet state is quenched completely before the 20 ns initial instrumental delay, or the singlet state is quenched before it can cross over into the triplet manifold. Having established the basic behavior of the dyes in water, an attempt was made to determine if the transient peak in the quenched OPE1 could be restored by titration with an oppositely charged surfactant, previously found to form strong complexes, shield the dye from water-based quenching and photodamage, and significantly affect the dye's behavior.[50,56,58] The TTA decay traces of OPE1 titrated with TTAB to a concentration just under CMC (1 mM for TTAB) are shown in Figure V.1. With the addition of TTAB, a transient peak at 600 nm is seen to appear with increasing intensity as more and more dye molecules are complexed and can reach their triplet state.
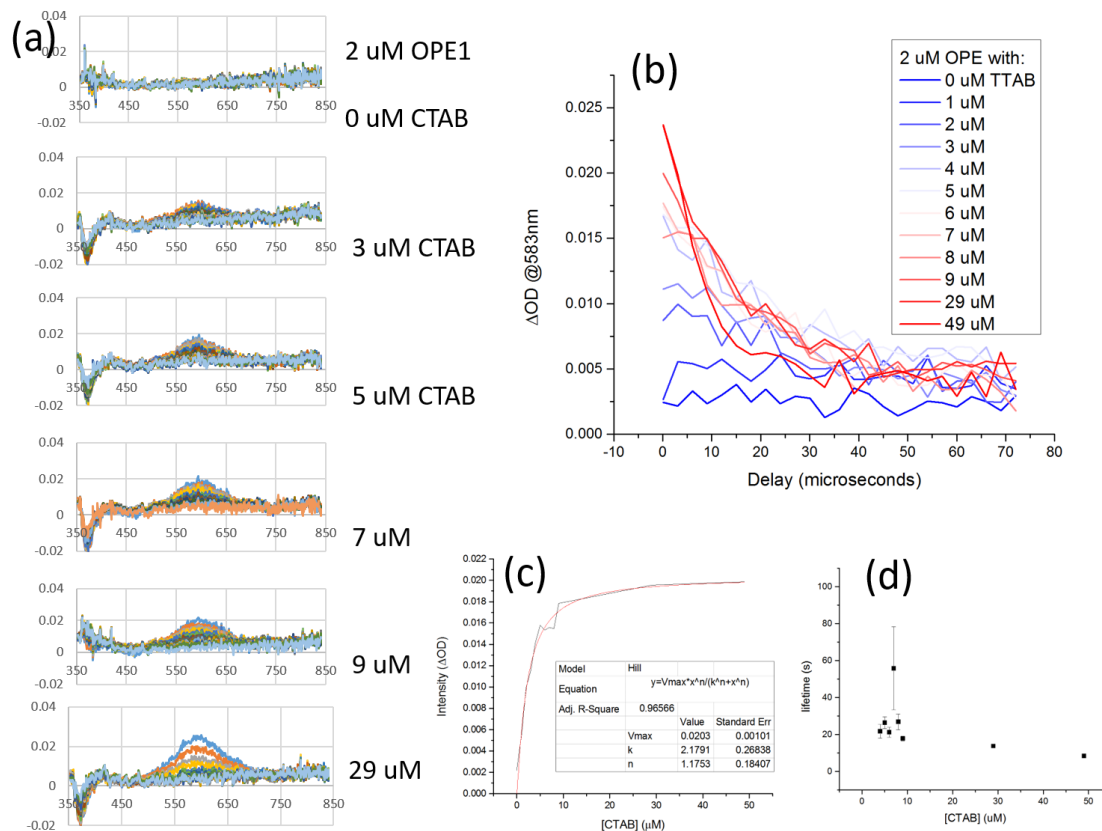
Figure V.2. Results of sub-micellar TTAB titration (0 to 49 uM) of 2 uM OPE1. (a): TTA traces, 35 ns initial delay, 3 us delay increment. (b): peak intensity at 583nm for each TTAB concentration plotted against delay time. (c): peak intensity at 3035 ns delay plotted against TTAB concentration, showing Langmuir-type binding saturation. (d): lifetime (from fitting of decay curves in figure V.2(b) to first-order kinetics) plotted against TTAB concentration, showing minor dependence of lifetime on TTAB concentration.

Just reaching the triplet state is not sufficient for the intended application, however. The OPE has not been shown to switchably generate singlet oxygen, or switchably enact photodamage to a living system of interest. The effects of random oxidation on particularly delicate systems are also an unknown factor. However, the present study has provided a proof of concept which can ground further investigation.

VI. Conclusions

This thesis has reported the results of four different studies into the synthesis, properties and behavior of oligo(p-phenylene ethynylene) electrolytes as tools for understanding and perturbing biological systems. The detailed investigation of the influence of different cationic groups on the effectiveness of photoactivated antimicrobials (Project 1) remains incomplete. A library of 18 functional dyes was evaluated against model amyloid proteins and OPE1 and OPE2 were identified as useful solution-phase dyes for amyloid and lead candidates for further evaluation (Project 2). The required properties for amyloid binding were determined to be steric and Coulombic targeting by a detailed balance of factors, and a desolvation-triggered fluorescence change mediated by solvent-interactive ethyl ester groups. OPE1 and OPE2 were used to stain amyloid-positive brain tissue and OPE1 behaved equally well as thioflavin T, but with some useful differences, while OPE2 exhibited unwanted binding elsewhere in the tissue (Project 3). Finally, the use of surfactant-mediated self-assembly to control the accessibility and population of triplet states in OPE organic dyes was investigated, and found to be a viable approach worthy of additional study (Project 4).

VII. Future Work

The future of research into these molecules is dependent on well-defined structure-property relationships for rational molecular design. Projects 1, 2 and 3 all were based around understanding the ways that molecular structure changes useful behavior in complex biological systems, and each produced some useful information that could guide further efforts. As indicated in Section III above, the solvent-sensitive emission property of the ester-conjugated OPEs was discovered by accident, and has not been satisfactorily explained in theoretical terms. Future workers could profit by understanding better how to control and improve the functionality of this particular effect.

Synthesis of a new series of analogues to the existing OPE fluorophores will produce: improved solvent-sensitive emitters, with either increased yield in the dequenched state or further suppressed yield in the quenched state; and/or meaningful structure-function relationships for the design of new hydrophobicity-sensing fluorescent dyes. "Turn-on" emission in response to analyte is commonly-held goal in studies of fluorescent sensing. Previous studies have mostly reported fluorogenesis resulting from forced planarization of an intramolecular rotor in the π system[81,82], while the emission changes of these OPEs are determined by the properties of the solvent. Structure-function relationships for fluorogenesis do not exist satisfactorily. Improving the fundamental understanding of fluorogens will have impact far beyond the specific sensing of amyloid; solvent-based fluorogenesis can be used to make flexible sensor systems based on a variety of self-assembly properties.

References

(1) Digman, M. A., and Gratton, E. (2009) Fluorescence correlation spectroscopy and fluorescence cross-correlation spectroscopy. *Wiley Interdiscip. Rev. Syst. Biol. Med. 1*, 273–282.

(2) Sahoo, H. (2011) F??rster resonance energy transfer - A spectroscopic nanoruler: Principle and applications. *J. Photochem. Photobiol. C Photochem. Rev. 12*, 20–30.

(3) Tani, T. (1995) Photographic Sensitivity : Theory and Mechanisms. Oxford University Press, USA, New York.

(4) Castano, A. P., Mroz, P., and Hamblin, M. R. (2006) Photodynamic therapy and anti-tumour immunity. *Nat. Rev. Cancer 6*, 535–45.

(5) Cepraga, C., Gallavardin, T., Marotte, S., Lanoë, P.-H., Mulatier, J.-C., Lerouge, F., Parola, S., Lindgren, M., Baldeck, P. L., Marvel, J., Maury, O., Monnereau, C., Favier, A., Andraud, C., Leverrier, Y., and Charreyre, M.-T. (2013) Biocompatible well-defined chromophore–polymer conjugates for photodynamic therapy and two-photon imaging. *Polym. Chem. 4*, 61.

(6) Kuimova, M. K., Collins, H. a, Balaz, M., Dahlstedt, E., Levitt, J. a, Sergent, N., Suhling, K., Drobizhev, M., Makarov, N. S., Rebane, A., Anderson, H. L., and Phillips, D. (2009) Photophysical properties and intracellular imaging of water-soluble porphyrin dimers for two-photon excited photodynamic therapy. *Org. Biomol. Chem. 7*, 889–96.

(7) Baptista, M. S., and Wainwright, M. (2011) Photodynamic antimicrobial chemotherapy (PACT) for the treatment of malaria, leishmaniasis and trypanosomiasis. *Brazilian J. Med. Biol. Res. 44*, 1–10.

(8) Wilde, K. N., Whitten, D. G., and Canavan, H. E. (2013) In vitro cytotoxicity of antimicrobial conjugated electrolytes: interactions with mammalian cells. *ACS Appl. Mater. Interfaces 5*, 9305–11.

(9) Parthasarathy, A., Pappas, H. C., Hill, E. H., Huang, Y., Whitten, D. G., and Schanze, K. S. (2015) Conjugated Polyelectrolytes with Imidazolium Solubilizing Groups. Properties and Application to Photodynamic Inactivation of Bacteria. *ACS Appl. Mater. Interfaces* 150616144031005.

(10) Ji, E., Corbitt, T. S., Parthasarathy, A., Schanze, K. S., and Whitten, D. G. (2011) Light and dark-activated biocidal activity of conjugated polyelectrolytes. *ACS Appl. Mater. Interfaces 3*, 2820–9.

(11) Wang, Y., Canady, T. D., Zhou, Z., Tang, Y., Price, D. N., Bear, D. G., Chi, E. Y., Schanze, K. S., and Whitten, D. G. (2011) Cationic phenylene ethynylene polymers and oligomers exhibit efficient antiviral activity. *ACS Appl. Mater. Interfaces 3*, 2209–14.

(12) Dascier, D., Ji, E., Parthasarathy, A., Schanze, K. S., and Whitten, D. G. (2012) Efficacy of end-only-functionalized oligo(arylene-ethynylene)s in killing bacterial biofilms. *Langmuir 28*, 11286–90.

(13) Wang, Y., Canady, T. D., Zhou, Z., Tang, Y., Price, D. N., Bear, D. G., Chi, E. Y., Schanze, K. S., and Whitten, D. G. (2011) Cationic phenylene ethynylene polymers and oligomers exhibit efficient antiviral activity. *ACS Appl. Mater. Interfaces 3*, 2209–14.

(14) Pappas, H. C., Sylejmani, R., Graus, M. S., Donabedian, P. L., Whitten, D. G., and Neumann, A. K. (2016) The Antifungal Properties of Cationic Phenylene Ethynylenes and their Impact on β-Glucan Exposure. *Antimicrob. Agents Chemother.*

(15) Zhou, Z., Corbitt, T. S., Parthasarathy, A., Tang, Y., Ista, L. K., Schanze, K. S., and Whitten, D. G. (2010) "End-Only" Functionalized Oligo(phenylene ethynylene)s: Synthesis, Photophysical and Biocidal Activity. *J. Phys. Chem. Lett. 1*, 3207–3212.

(16) Tang, Y., Hill, E. H., Zhou, Z., Evans, D. G., Schanze, K. S., and Whitten, D. G. (2011) Synthesis, Self-Assembly, and Photophysical Properties of Cationic Oligo(p -phenyleneethynylene)s. *Langmuir 27*, 4945–4955.

(17) Ittner, L. M., and Götz, J. (2011) Amyloid-β and tau--a toxic pas de deux in Alzheimer's disease. *Nat. Rev. Neurosci. 12*, 65–72.

(18) Knowles, T. P. J., Vendruscolo, M., and Dobson, C. M. (2014) The amyloid state and its association with protein misfolding diseases. *Nat. Rev. Mol. Cell Biol. 15*, 384–96.

(19) Eisenberg, D., and Jucker, M. (2012) The amyloid state of proteins in human diseases. *Cell 148*, 1188–1203.

(20) Barnhart, M. M., and Chapman, M. R. (2006) Curli biogenesis and function. *Annu. Rev. Microbiol. 60*, 131–147.

(21) Nilsson, K. P. R., Ikenberg, K., Aslund, A., Fransson, S., Konradsson, P., Röcken, C., Moch, H., and

Aguzzi, A. (2010) Structural typing of systemic amyloidoses by luminescent-conjugated polymer spectroscopy. *Am. J. Pathol. 176*, 563–74.

(22) Sigurdson, C. C. J., Bartz, J. C. J., and Nilsson, K. P. R. (2011) Tracking protein aggregate interactions. *Prion 5*, 52–55.

(23) Johnson, K. a, Fox, N. C., Sperling, R. a, and Klunk, W. E. (2012) Brain imaging in Alzheimer disease. *Cold Spring Harb. Perspect. Med. 2*, a006213.

(24) De Genst, E., Messer, A., and Dobson, C. M. (2014) Antibodies and protein misfolding: From structural research tools to therapeutic strategies. *Biochim. Biophys. Acta 1844*, 1907–1919.

(25) Jack, C. R., Barrio, J. R., and Kepe, V. (2013) Cerebral amyloid PET imaging in Alzheimer's disease. *Acta Neuropathol. 126*, 643–57.

(26) Amiri, H., Saeidi, K., Borhani, P., Manafirad, A., Ghavami, M., and Zerbi, V. (2013) Alzheimer's disease: pathophysiology and applications of magnetic nanoparticles as MRI theranostic agents. *ACS Chem. Neurosci. 4*, 1417–29.

(27) Skeby, K. K., Sørensen, J., and Schiøtt, B. (2013) Identification of a Common Binding Mode for Imaging Agents to Amyloid Fibrils from Molecular Dynamics Simulations. *J. Am. Chem. Soc. 135*, 15114–15128.

(28) Mao, X., Guo, Y., Wang, C., Zhang, M., Ma, X., Liu, L., Niu, L., Zeng, Q., Yang, Y., and Wang, C. (2011) Binding modes of thioflavin T molecules to prion peptide assemblies identified by using scanning tunneling microscopy. *ACS Chem. Neurosci. 2*, 281–287.

(29) Nilsson, K. P. R. (2009) Small organic probes as amyloid specific ligands--past and recent molecular scaffolds. *FEBS Lett. 583*, 2593–9.

(30) Zhang, X., Tian, Y., Yuan, P., Li, Y., Yaseen, M. a, Grutzendler, J., Moore, A., and Ran, C. (2014) A bifunctional curcumin analogue for two-photon imaging and inhibiting crosslinking of amyloid beta in Alzheimer's disease. *Chem. Commun. (Camb). 50*, 11550–3.

(31) Zhang, X., Tian, Y., Li, Z., Tian, X., Sun, H., Liu, H., Moore, A., and Ran, C. (2013) Design and synthesis of curcumin analogues for in vivo fluorescence imaging and inhibiting copper-induced cross-linking of amyloid beta species in Alzheimer's disease. *J. Am. Chem. Soc. 135*, 16397–409.

(32) Cui, M., Ono, M., Kimura, H., Liu, B., and Saji, H. (2011) Synthesis and structure-affinity relationships of novel dibenzylideneacetone derivatives as probes for β-amyloid plaques. *J. Med. Chem. 54*, 2225–40.

(33) Ono, M., Kawashima, H., Nonaka, A., Kawai, T., Haratake, M., Mori, H., Kung, M. P., Kung, H. F., Saji, H., and Nakayama, M. (2006) Novel benzofuran derivatives for PET imaging of β-amyloid plaques in Alzheimer's disease brains. *J. Med. Chem. 49*, 2725–2730.

(34) Harrison, S. T., Mulhearn, J., Wolkenberg, S. E., Miller, P. J., O'Malley, S. S., Zeng, Z., Williams, D. L., Hostetler, E. D., Sanabria-Bohórquez, S., Gammage, L., Fan, H., Sur, C., Culberson, J. C., Hargreaves, R. J., Cook, J. J., Hartman, G. D., and Barrow, J. C. (2011) Synthesis and Evaluation of 5-Fluoro-2-aryloxazolo[5,4-b]pyridines as β-Amyloid PET Ligands and Identification of MK-3328. *ACS Med. Chem. Lett. 2*, 498–502.

(35) Yoshimura, M., Ono, M., Matsumura, K., Watanabe, H., Kimura, H., Cui, M., Nakamoto, Y., Togashi, K., Okamoto, Y., Ihara, M., Takahashi, R., and Saji, H. (2013) Structure-Activity Relationships and in Vivo Evaluation of Quinoxaline Derivatives for PET Imaging of β-Amyloid Plaques. *ACS Med. Chem. Lett. 4*, 596–600.

(36) Herland, A., Nilsson, K. P. R., Olsson, J. D. M., Hammarström, P., Konradsson, P., and Inganäs, O. (2005) Synthesis of a regioregular zwitterionic conjugated oligoelectrolyte, usable as an optical probe for detection of amyloid fibril formation at acidic pH. *J. Am. Chem. Soc. 127*, 2317–23.

(37) Arja, K., Sjölander, D., Åslund, A., Prokop, S., Heppner, F. L., Konradsson, P., Lindgren, M., Hammarström, P., Åslund, K. O. A., and Nilsson, K. P. R. (2013) Enhanced fluorescent assignment of protein aggregates by an oligothiophene-porphyrin-based amyloid ligand. *Macromol. Rapid Commun. 34*, 723–30.

(38) Klingstedt, T., Shirani, H., Åslund, K. O. A., Cairns, N. J., Sigurdson, C. J., Goedert, M., and Nilsson, K. P. R. (2013) The structural basis for optimal performance of oligothiophene-based fluorescent amyloid ligands: Conformational flexibility is essential for spectral assignment of a diversity of protein aggregates. *Chem. - A Eur. J. 19*, 10179–10192.

(39) Ries, J., Udayar, V., Soragni, A., Hornemann, S., Nilsson, K. P. R., Riek, R., Hock, C., Ewers, H., Aguzzi, A. a, and Rajendran, L. (2013) Superresolution imaging of amyloid fibrils with binding-activated probes. *ACS Chem. Neurosci. 4*, 1057–61.

(40) Klingstedt, T., Aslund, A., Simon, R. a, Johansson, L. B. G., Mason, J. J., Nyström, S., Hammarström, P., and Nilsson, K. P. R. (2011) Synthesis of a library of oligothiophenes and their utilization as fluorescent ligands for spectral assignment of protein aggregates. *Org. Biomol. Chem. 9*, 8356–70.

(41) Aslund, A., Sigurdson, C. J., Klingstedt, T., Grathwohl, S., Bolmont, T., Dickstein, D. L., Glimsdal, E., Prokop, S., Lindgren, M., Konradsson, P., Holtzman, D. M., Hof, P. R., Heppner, F. L., Gandy, S., Jucker, M., Aguzzi, A., Hammarström, P., and Nilsson, K. P. R. (2009) Novel pentameric thiophene derivatives for in vitro and in vivo optical imaging of a plethora of protein aggregates in cerebral amyloidoses. *ACS Chem. Biol. 4*, 673–84.

(42) Ono, M., Watanabe, H., Kimura, H., and Saji, H. (2012) BODIPY-Based Molecular Probe for Imaging of Cerebral β-Amyloid Plaques. *ACS Chem. Neurosci. 3*, 319–324.

(43) Chang, W. M., Dakanali, M., Capule, C. C., Sigurdson, C. J., Yang, J., and Theodorakis, E. A. (2011) ANCA: A Family of Fluorescent Probes that Bind and Stain Amyloid Plaques in Human Tissue. *ACS Chem. Neurosci. 2*, 249–255.

(44) Cui, M., Ono, M., Watanabe, H., Kimura, H., Liu, B., and Saji, H. (2014) Smart near-infrared fluorescence probes with donor-acceptor structure for in vivo detection of β-amyloid deposits. *J. Am. Chem. Soc. 136*, 3388–94.

(45) Tang, Y., Hill, E. H., Zhou, Z., Evans, D. G., Schanze, K. S., and Whitten, D. G. (2011) Synthesis, self-assembly, and photophysical properties of cationic oligo(p-phenyleneethynylene)s. *Langmuir 27*, 4945–55.

(46) Hill, E. H., Zhang, Y., Evans, D. G., and Whitten, D. G. (2015) Enzyme-Specific Sensors via Aggregation of Charged *p*- Phenylene Ethynylenes. *ACS Appl. Mater. Interfaces 7*, 5550–5560.

(47) Wang, Y., Schanze, K. S., Chi, E. Y., and Whitten, D. G. (2013) When worlds collide: interactions at the interface between biological systems and synthetic cationic conjugated polyelectrolytes and oligomers. *Langmuir 29*, 10635–47.

(48) Liu, Y., Ogawa, K., and Schanze, K. S. (2009) Conjugated polyelectrolytes as fluorescent sensors. *J. Photochem. Photobiol. C Photochem. Rev. 10*, 173–190.

(49) Wang, Y., Jett, S. D., Crum, J., Schanze, K. S., Chi, E. Y., and Whitten, D. G. (2013) Understanding the dark and light-enhanced bactericidal action of cationic conjugated polyelectrolytes and oligomers. *Langmuir 29*, 781–92.

(50) Hill, E. H., Pappas, H. C., and Whitten, D. G. (2014) Activating the antimicrobial activity of an anionic singlet-oxygen sensitizer through surfactant complexation. *Langmuir 30*, 5052–6.

(51) Corbitt, T. S., Sommer, J. R., Chemburu, S., Ogawa, K., Ista, L. K., Lopez, G. P., Whitten, D. G., and Schanze, K. S. (2009) Conjugated polyelectrolyte capsules: light-activated antimicrobial micro "Roach Motels". *ACS Appl. Mater. Interfaces 1*, 48–52.

(52) Pinto, M. R., and Schanze, K. S. (2004) Amplified fluorescence sensing of protease activity with conjugated polyelectrolytes. *Proc. Natl. Acad. Sci. U. S. A. 101*, 7505–10.

(53) An, L., Liu, L., and Wang, S. (2009) Label-free, homogeneous, and fluorescence "turn-on" detection of protease using conjugated polyelectrolytes. *Biomacromolecules 10*, 454–7.

(54) Kushon, S. A., Ley, K. D., Bradford, K., Jones, R. M., McBranch, D., and Whitten, D. (2002) Detection of DNA hybridization via fluorescent polymer superquenching. *Langmuir 18*, 7245–7249.

(55) Liu, Y., Ogawa, K., and Schanze, K. S. (2008) Conjugated polyelectrolyte based real-time fluorescence assay for phospholipase C. *Anal. Chem. 80*, 150–8.

(56) Hill, E. H., Sanchez, D., Evans, D. G., and Whitten, D. G. (2013) Structural basis for aggregation mode of oligo-p-phenylene ethynylenes with ionic surfactants. *Langmuir 29*, 15732–7.

(57) Würthner, F., Kaiser, T. E., and Saha-Möller, C. R. (2011) J-aggregates: from serendipitous discovery to supramolecular engineering of functional dye materials. *Angew. Chem. Int. Ed. Engl. 50*, 3376–410.

(58) Hill, E. H., Evans, D. G., and Whitten, D. G. (2014) The influence of structured interfacial water on the photoluminescence of carboxyester-terminated oligo-p-phenylene ethynylenes. *J. Phys. Org. Chem. 27*, 252–257.

(59) Swaminathan, R., Ravi, V. K., Kumar, S., Kumar, M. V. S., and Chandra, N. (2011) Lysozyme: A model protein for amyloid research. *Adv. Protein Chem. Struct. Biol. 84*, 63–111.

(60) Gharibyan, A. L., Zamotin, V., Yanamandra, K., Moskaleva, O. S., Margulis, B. a, Kostanyan, I. a, and Morozova-Roche, L. a. (2007) Lysozyme amyloid oligomers and fibrils induce cellular death via different apoptotic/necrotic pathways. *J. Mol. Biol. 365*, 1337–49.

(61) Mulaj, M., Foley, J., and Muschol, M. (2014) Amyloid oligomers and protofibrils, but not filaments, self-replicate from native lysozyme. *J. Am. Chem. Soc. 136*, 8947–56.

(62) Greenfield, N. (2007) Using circular dichroism spectra to estimate protein secondary structure. *Nat. Protoc. 1*, 2876–2890.

(63) Goutelle, S., Maurin, M., Rougier, F., Barbaut, X., Bourguignon, L., Ducher, M., and Maire, P. (2008) The Hill equation: A review of its capabilities in pharmacological modelling. *Fundam. Clin. Pharmacol. 22*, 633–648.

(64) Kim, I., Dunkhorst, A., and Bunz, U. H. F. (2005) Nonspecific interactions of a carboxylate-substituted PPE with proteins. A cautionary tale for biosensor applications. *Langmuir 21*, 7985–9.

(65) Piston, D. W., and Kremers, G.-J. (2007) Fluorescent protein FRET: the good, the bad and the ugly. *Trends Biochem. Sci. 32*, 407–414.

(66) Neef, D., and Walling, A. D. (2006) Dementia with Lewy bodies: An emerging disease. *Am. Fam. Physician 73*, 1223–1230.

(67) Ahmad, a., Uversky, V. N., Hong, D., and Fink, a. L. (2005) Early Events in the Fibrillation of Monomeric Insulin. *J. Biol. Chem. 280*, 42669–42675.

(68) Shih, P., Holland, D. R., and Kirsch, J. F. (1995) Thermal stability determinants of chicken egg-white lysozyme core mutants: hydrophobicity, packing volume, and conserved buried water molecules. *Protein Sci. 4*, 2050–2062.

(69) Amdursky, N., Erez, Y., and Huppert, D. (2012) Molecular rotors: What lies behind the high sensitivity of the thioflavin-T fluorescent marker. *Acc. Chem. Res. 45*, 1548–1557.

(70) Wu, J. W., Liu, K.-N., How, S.-C., Chen, W.-A., Lai, C.-M., Liu, H.-S., Hu, C.-J., and Wang, S. S.-S. (2013) Carnosine's effect on amyloid fibril formation and induced cytotoxicity of lysozyme. *PLoS One 8*, e81982.

(71) Nielsen, L., Khurana, R., Coats, A., Frokjaer, S., Brange, J., Vyas, S., Uversky, V. N., and Fink, A. L. (2001) Effect of Environmental Factors on the Kinetics of Insulin Fibril Formation: Elucidation of the Molecular Mechanism †. *Biochemistry 40*, 6036–6046.

(72) James, P. V, Sudeep, P. K., Suresh, C. H., and Thomas, K. G. (2006) Photophysical and Theoretical Investigations of Oligo (p -phenyleneethynylene) s : Effect of Alkoxy Substitution and Alkyne - Aryl Bond Rotations 4329–4337.

(73) Fleming, G. R., Knight, A. E. W., Morris, J. M., Robbins, R. J., and Robinson, G. W. (1977) Slip Boundary-Conditions for Molecular Rotation - Time-Dependent Fluorescence Depolarization Studies of Bbot. *Chem. Phys. Lett. 51*, 399–402.

(74) Nambiar, R., Woody, K. B., Ochocki, J. D., Brizius, G. L., and Collard, D. M. (2009) Synthetic Approaches to Regioregular Unsymmetrical Dialkoxy-Substituted Poly(1,4-phenylene ethynylene)s. *Macromolecules 42*, 43–51.

(75) Lamb, B. T., Bardel, K. A., Laura, S., Anderson, J. J., Holtz, G., Steven, L., Sisodia, S. S., and Hoeger, E. J. (1999) Amyloid production and deposition in mutant amyloid precursor protein and presenilin-1 yeast artificial chromosome transgenic mice *40*, 695–697.

(76) Santacruz, K., Lewis, J., Spires, T., Paulson, J., Kotilinek, L., Ingelsson, M., Guimaraes, A., DeTure, M., Ramsden, M., McGowan, E., Forster, C., Yue, M., Orne, J., Janus, C., Mariash, A., Kuskowski, M., Hyman, B., Hutton, M., and Ashe, K. H. (2005) Tau suppression in a neurodegenerative mouse model improves memory function. *Science 309*, 476–81.

(77) Allison, R. R., and Sibata, C. H. (2010) Oncologic photodynamic therapy photosensitizers: A clinical review. *Photodiagnosis Photodyn. Ther. 7*, 61–75.

(78) Tang, Y., Zhou, Z., Ogawa, K., Lopez, G. P., Schanze, K. S., and Whitten, D. G. (2009) Photophysics and self-assembly of symmetrical and unsymmetrical cationic oligophenylene ethynylenes. *J. Photochem. Photobiol. A Chem. 207*, 4–6.

(79) Wang, Y., Tang, Y., Zhou, Z., Ji, E., Lopez, G. P., Chi, E. Y., Schanze, K. S., and Whitten, D. G. (2010) Membrane perturbation activity of cationic phenylene ethynylene oligomers and polymers: selectivity against model bacterial and mammalian membranes. *Langmuir 26*, 12509–14.

(80) Wasserberg, D. Triplet States – Triplet Fates. Technical University Eindhoven.

(81) Wu, J., Liu, W., Ge, J., Zhang, H., and Wang, P. (2011) New sensing mechanisms for design of fluorescent chemosensors emerging in recent years. *Chem. Soc. Rev. 40*, 3483–3495.

(82) Hong, Y., Lam, J. W. Y., and Tang, B. Z. (2011) Aggregation-induced emission. *Chem. Soc. Rev. 40*, 5361.